Random square-triangle tilings: A model for twelvefold-symmetric quasicrystals

Mark Oxborrow* and Christopher L. Henley
Laboratory of Atomic and Solid State Physics, Cornell University, Ithaca, New York 14853-2501
(Received 17 June 1992)

Random tilings that comprise squares and equilateral triangles can model quasicrystals with twelvefold symmetry. A (phason) elastic theory for such tilings is constructed, whose order parameter is the phason field, and whose entropy density includes terms up to third order in the phason strain. Due to an unusual constraint, the phason field of any square-triangle tiling is irrotational and, as a result, the form of the entropy density is simpler than the general form that is required by twelvefold symmetry alone. Using an update move, which rearranges a closed, nonlocal, one-dimensional chain of squares and triangles, the unknown parameters of the elastic theory are estimated via Monte Carlo simulations: (i) One of the two second-order elastic constants and the third-order elastic constant are found by measuring phason fluctuations; athermal systems (maximally random ensembles) with the same background phason strain but different sizes of unit cell are simulated to distinguish the effects of a finite background phason strain from the effects of finite unit-cell size. (ii) The entropy per unit area at zero phason strain and the other second-order elastic constant are found from the entropies that thermal systems (canonical ensembles) gain between zero and infinite temperature, which are estimated using Ferrenberg and Swendsen's histogram method. A way to set up transfer-matrix calculations for random square-triangle tilings is also presented.

I. INTRODUCTION

Why do quasicrystals[1] exist? A reasonable yet contentious postulate is that a quasicrystal is a thermodynamic system, in equilibrium, whose free energy depends on the temperature, the *phason strain*,[2] and other macroscopic variables. If this conceptual framework is adopted, the above question becomes: Why does a quasicrystal's free energy, as a function of the above variables, exhibit a minimum about zero phason strain? A *random-tiling model*[2,3] is a maximally random ensemble that comprises random tilings. Under a suitably formulated *decoration scheme*,[4] every such tiling corresponds to an atomic structure. A random-tiling model plus a decoration scheme constitutes a *physical model* that specifies, in a statistical sense, the atomic structure of a (random) quasicrystal. By design, a model of this sort supplies the latter question (above) with a definite answer: The entropy that arises from coordinated atomic relocations, where each such relocation is equivalent (under the decoration scheme) to a rearrangement of tiles, causes the model's free energy to exhibit a minimum where the phason strain vanishes.

The prose of this paper contains various technical words, specific to either quasicrystals, random-tiling models, or Monte Carlo algorithmics, whose use facilitates succinct expression. As a service and/or warning to the reader, each such word is italicized, either where it first appears or where it is explicitly defined, or both. To reduce, in this paper, the number of those instances where a technical word is—by necessity—used before it is defined, the meanings of some technical words are laid out forthwith, in a logical sequence: The verbs *to comprise* and *to compose* express set-theoretical relationships; if A comprises B and C, then both (i) A contains B, but A does not comprise B, and (ii) B and C compose A, but B alone does not. Every *triangle* is equilateral [this default makes sense because nonequilateral triangles (isosceles, scalene, ...) are nowhere mentioned in this paper]. A *square-triangle* tiling comprises squares and triangles (that is, it contains exclusively squares and triangles). A *unit cell* is a region, whose sides are subject to periodic boundary conditions. An *approximant* is a tiling that tiles a unit cell. An *ensemble* comprises *members*, which *occur* with certain *probabilities*. A *system* is the (physical) embodiment of an ensemble.[5] An ensemble *of* (random) tilings has, as an attribute, certain boundary conditions; unless stated otherwise, the ensemble comprises every tiling that satisfies these boundary conditions; in this sense, an ensemble of (random) tilings is a function of its boundary conditions. A *random* tiling is a generic member of such an ensemble. The members of a *maximally random* ensemble occur with equal probabilities. Hence, a canonical ensemble (in Gibbs' sense of the adjective "canonical") is maximally random if either its temperature is infinite or its Hamiltonian is zero. An *estimate* is a *best value* plus or minus a *random error*. The manifold meaning of the word "random" is unfortunate, but, due to historical precedent, somewhat unavoidable.

This paragraph is devoted to the definition of a single technical word. *Zipper*:[6] a rearrangement affecting an indefinite number of sites in a random tiling (or similar statistical geometry), which can be effected only by creating a pair of defects and propagating each defect along a path, such that along each path the tiling is changed (but would be restored if the path were retraced), until the defects annihilate. (A zipper of squares and triangles is illustrated below by Fig. 3.) This word represents a unifying concept (zippers can occur in both two-dimensional

0163-1829/93/48(10)/6966(33)/$06.00

and three-dimensional random tilings). Its use shortens the length of this paper by several pages. A "zipper" is, henceforth, a zipper of squares and triangles unless stated otherwise.

This paper is about maximally random ensembles that comprise square-triangle tilings. See Fig. 1. Though infinite random square-triangle tilings have 12-fold symmetry,[7] this symmetry alone determines only some of the qualitative properties, and none of the quantitative properties, that random square-triangle tilings exhibit. In the thermodynamic (infinite-system) limit, the statistical behavior of random square-triangle tilings can be described (for small background phason strains) by an *entropy density* that contains just a few unknown parameters: two second-order elastic constants, one third-order elastic constant, and the entropy per unit area (or equivalently the entropy per vertex) at zero phason strain. This paper describes various Monte Carlo methods, which were used to estimate these parameters and which were all based on an *update move* that effects a zipper.

Tang,[8] Shaw, Elser, and Henley,[9] and Strandburg[10] successfully studied ensembles of random three-dimensional Penrose tilings via Monte Carlo simulations, which were all based on a (local) update move that *flips* a rhombic dodecahedron comprising two oblate and two prolate rhombohedra. Various physical models for icosahedral quasicrystals, which all use random three-dimensional Penrose tilings as their geometrical framework(s), have been proposed.[11–13] Each of them, however, is unsatisfactory in at least one aspect: For the model proposed in Ref. 11, not every tiling corresponds to a *good*[14] atomic structure; around certain vertices the local density of atoms is too high. For the models proposed in Refs. 12 and 13, many atomic structures are excluded that could be as good as the ones allowed; no natural selection criterion is apparent.

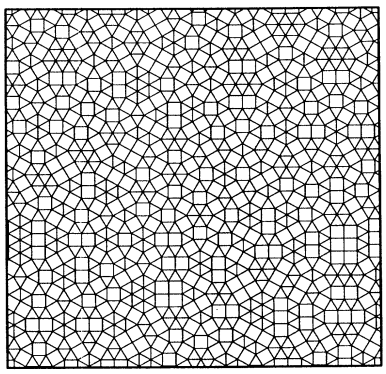

FIG. 1. Random square-triangle tiling (a non-Stampfli [2, 2]-type square-triangle approximant (see Sec. V C), containing $N_v = 836$ vertices, with a side length $L = 2(2 + \sqrt{3})^2 \approx 27.8564$); interpenetrating and fused dodecagons, which do not appear in Stampfli tilings, are also found in Ref. 97, Fig. 2 [a high-resolution electron-microscope image of a V-Ni(-Si) alloy].

Physical models that are based on ensembles of *canonical-cell* tilings[15] avoid the above problems: Every tiling corresponds to a good atomic structure; no equally good structures are excluded.[16] An update move for random canonical-cell tilings effects a zipper of canonical cells[17] (no *adequate*[18] update move that merely flips a small cluster of canonical cells is known). At present, neither an *acceptance region* nor an *inflation rule* is known for canonical-cell tilings; canonical-cell approximants that correspond to small background phason strains (such approximants are requisite for meaningful Monte Carlo simulations) cannot be built efficiently. But square-triangle tilings are the two-dimensional analogs of canonical cells: An adequate update move for random square-triangle tilings (see Sec. IV) effects a zipper of squares and triangles; this update move, by being what it is (a zipper), is qualitatively similar to a zipper of canonical cells. Because an inflation rule for square-triangle tilings is known,[19] moreover, square-triangle approximants that correspond to small background phason strains can be built easily. The study of random square-triangle tilings thus provides a two-dimensional arena for the development of all the tools and skills necessary to study ensembles that comprise canonical-cell tilings via Monte Carlo simulations successfully.

This paper is organized as follows: Section II first defines how a square-triangle tiling can be viewed as the projection of a two-dimensional representative surface that spans a four-dimensional regular lattice, then explains the irrotational property that all such representative surfaces exhibit. Section III presents a continuum (elastic) theory for ensembles of random square-triangle tilings; this theory involves an entropy density that contains an unknown entropy per unit area and unknown elastic constants. Section IV formulates an update move for random square-triangle tilings and discusses whether or not this update move *connects*[20] arbitrary random square-triangle tilings. Section V describes the random-Stampfli inflation rule, computes the entropy per vertex of infinite random-Stampfli tilings (at zero phason strain), then defines the random-Stampfli approximants that served as the starting configurations of Monte Carlo runs. Section VI details the (athermal) Monte Carlo simulations that were used to estimate one of the two second-order elastic constants and the (one and only) third-order elastic constant. Section VII motivates then details the (thermal) Monte Carlo simulations that were used to estimate the entropy per unit area at zero phason strain and the other second-order elastic constant. Section VIII formulates a transfer-matrix method for random square-triangle tilings and discusses the properties of the transfer matrices that this method engenders. Section IX, the conclusion, supplies a brief summary of results, catalogs the questions that remain unanswered, mentions the experimental (three-dimensional) systems that are related to (random) square-triangle tilings and considers in more detail the implementation of Monte Carlo simulations for random canonical-cell tilings. Appendix A contains a derivation of the general form, up to third order in the phason strain, that a 12-fold-symmetric entropy density takes (the form is quoted in Sec. III B).

Appendix B supplies proofs of detailed balance that are omitted from Secs. VI A and VII D. Appendix C outlines an alternative [viz., Ma's coincidence-counting (Monte Carlo) method] to the Monte Carlo method (viz., the pseudo-Hamiltonian–histogram method) that is detailed in Secs. VII B–VII F.

A paper's introduction should both (i) allow readers to ascertain what they can gain by studying the paper and (ii) advise readers as to how they can gain whatever it is, without needless intellectual expenditure; this paragraph concerns both of these functions. Through necessity, this paper sets forth many definitions, much notation, and toils over numerous technical details. Readers for whom this is their first exposure to random-tiling models should start by not reading any further; rather, they should peruse Henley's recent review article (Ref. 2), or its equivalent. Readers for whom this is their second or third exposure to random-tiling models should begin by working through Secs. II and III in a methodical fashion. And readers for whom this is their nth exposure to random-tiling models should jump straight to Sec. IX A, which summarizes and locates the significant results that this paper contains, then proceed to tackle whatever else, wherever in the paper it happens to be.

II. PRELIMINARIES

In what follows, the language through which this paper describes the properties of square-triangle tilings is defined. A square-triangle tiling can be viewed as the projection of a *representative surface* onto a two-dimensional *parallel* (a.k.a. physical or real) *space*, where the representative surface is two-dimensional yet spans a four-dimensional regular lattice. References 2 and 21 contain illustrations that make clear the simple yet fundamental idea mental picture, ubiquitous in descriptions of quasicrystals, which the words of the previous sentence imply. Section II A defines the representative surface of a square-triangle tiling. Section II B explains the irrotational property that the representative surfaces of all such tilings exhibit.

A. Square-triangle tilings in four dimensions

The representative surface of a square-triangle tiling comprises a subset of the two-dimensional faces that bound the (four-dimensional) cells of a four-dimensional regular lattice. This lattice is generated by four basis vectors $\{\mathbf{e}_0,\ldots,\mathbf{e}_3\}$, where $\{\mathbf{e}_0,\mathbf{e}_2\}$ and $\{\mathbf{e}_1,\mathbf{e}_3\}$ generate mutually orthogonal, two-dimensional (regular) triangular sublattices. Designating a vertex of the four-dimensional lattice to serve as an origin, the parallel-space position vector of a vertex v in a square-triangle tiling can be expressed as

$$\mathbf{r}_v = \sum_{i=0}^{3} n_i \mathbf{e}_i^{\parallel}, \tag{1}$$

where $n_0,\ldots,n_3$ are four (unique) integers, and $\{\mathbf{e}_0^{\parallel},\ldots,\mathbf{e}_3^{\parallel}\}$ are the projections of $\{\mathbf{e}_0,\ldots,\mathbf{e}_3\}$ onto the two-dimensional parallel space. In Cartesian-component form, these projections are

$$\mathbf{e}_i^{\parallel} = (\cos[\alpha i],\sin[\alpha i])^{\parallel}, \tag{2}$$

where $i \in \{0,\ldots,3\}$ and $\alpha = \pi/6$. See Fig. 2(a). (Note that $|\mathbf{e}_i^{\parallel}| = 1$; i.e., squares and triangles have unit side length.) Similarly, the projections of $\{\mathbf{e}_0,\ldots,\mathbf{e}_3\}$ onto the two-dimensional *perpendicular* (henceforth *perp.*) *space*, which lies orthogonal to the parallel space, are[22]

$$\mathbf{e}_i^{\perp} = (\cos[7\alpha i],\sin[7\alpha i])^{\perp}. \tag{3}$$

See Fig. 2(b). The perp.-space position vector of the (above) vertex v is defined as

$$\mathbf{f}_v = \sum_{i=0}^{3} n_i \mathbf{e}_i^{\perp}, \tag{4}$$

where the n_i are the same n_i as appear in Eq. (1). The four-dimensional position vector of the vertex v is $\mathbf{r}_v \oplus \mathbf{f}_v$.

Consider the point on the representative surface of a square-triangle tiling that corresponds to an arbitrary parallel-space position vector $\mathbf{r} = (r_1,r_2)^{\parallel}$. The perp.-space position vector $\mathbf{f} = (f_1,f_2)^{\perp}$ that corresponds to this point is defined by linearly interpolating (a two-dimensional face is flat) the perp.-space position vectors $(\mathbf{f}_v)$ of the vertices that lie at the corners of the tile that covers $\mathbf{r}$. This prescription defines the representative surface of a square-triangle tiling as a continuous function (a vector field), whose domain is parallel space and whose range is perp. space: $\mathbf{f}(\mathbf{r}) = (f_1(\mathbf{r}),f_2(\mathbf{r}))^{\perp}$.

B. Irrotational property: Tiles as topological charges

The representative surface of a (any) square-triangle tiling has the unusual property

$$\frac{\partial f_1}{\partial r_2} - \frac{\partial f_2}{\partial r_1} = 0, \tag{5}$$

for any $\mathbf{r}$. To translate Eq. (5) into words, the represen-

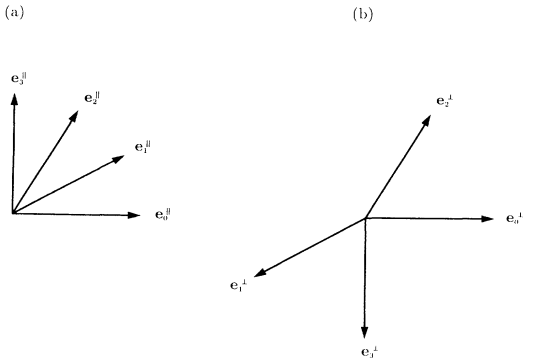

FIG. 2. Projections of the four four-dimensional primitive translation vectors (a) onto parallel space and (b) onto perp. space.

tative surface $\mathbf{f}(\mathbf{r})$ is irrotational. Equation (5) can be verified by explicitly evaluating its left-hand side, using Eqs. (2) and (3), for the parallel-space positions that lie within a square (for each of its three distinct orientations) and for the parallel-space positions that lie within a triangle (for each of its four distinct orientations). The integral-form equivalent of Eq. (5) is

$$\oint [f_1\, dr_1 + f_2\, dr_2] \equiv \oint \mathbf{f}(\mathbf{r}) \cdot d\mathbf{r} = 0, \tag{6}$$

where the line of integration is any closed path in parallel space. Because $\mathbf{f}(\mathbf{r})$ is irrotational, it can be expressed as the gradient of a scalar-potential field:

$$\mathbf{f}(\mathbf{r}) = \nabla \Phi(\mathbf{r}). \tag{7}$$

The concept of *topological charge* provides an interpretation of Eqs. (5)–(7). Define the topological charge $Q_{\mathcal{R}}$ that lies within a region of parallel space $\mathcal{R}$ to be

$$Q_{\mathcal{R}} = \oint_{\mathcal{R}} \mathbf{f}(\mathbf{r}) \cdot d\mathbf{r}, \tag{8}$$

where the line of integration bounds the region $\mathcal{R}$. Using Eqs. (1)–(4) above, the reader is asked to show that $Q_{\mathcal{R}}$ equals zero if the region $\mathcal{R}$ is either a square (in any of its three orientations) or a triangle (in any of its four orientations); the exercise is straightforward. This result implies that squares and triangles carry no topological charge. A tiling that comprises squares and triangles thus nowhere contains topological charge, and as a result, its representative surface is, everywhere, irrotational. Tilings that comprise squares, triangles, and thin (30°) rhombi,[25] however, are not irrotational; this is because each thin rhombus carries a nonzero topological charge, equal to $\pm\sqrt{3}$, the sign being dependent on the rhombus' orientation.

III. CONTINUUM THEORY

In what follows, a continuum (phason) elastic theory is constructed that describes maximally random (sub)ensembles of (random) square-triangle tilings at small but non-negligible background phason strains. The order parameter of the theory is the (modified) phason field, which is a coarse-grained version of the representative surface (Sec. II A). The entropy density of the theory contains products of (modified) phason-strain components, up to third order in the phason strain, which are multiplied by unknown (phenomenological) elastic constants. Through Eq. (38) below, two of these elastic constants are related to phason-mode fluctuations, whose magnitudes determine the sharpness of diffraction peaks for atomic models that are based on random square-triangle tilings. This connection between elastic constants and diffraction peaks[26] motivates, in part, the Monte Carlo simulations that were performed (Secs. VI and VII), whereby estimates of the elastic constants (Table III below) were obtained.

A. Coarse graining

The *phason field* of an infinite square-triangle tiling is defined as a convolution:

$$\mathbf{h}(\mathbf{r}) = (h_1(\mathbf{r}), h_2(\mathbf{r}))^{\perp} = \int \mathbf{f}(\mathbf{r}')\, \mathcal{W}(\mathbf{r}' - \mathbf{r})\, d^2\mathbf{r}'; \tag{9}$$

$\mathbf{f}(\mathbf{r})$ is the representative surface of the infinite square-triangle tiling; $\mathcal{W}(\mathbf{r})$ is a *weighting kernel*[27] that is both (i) smooth and (ii) normalized [i.e., $\int \mathcal{W}(\mathbf{r}')\, d^2\mathbf{r}' = 1$] and that (iii) varies on a characteristic length scale (width) $\Lambda \gg 1$ (a tile edge has unit length). Because of the smoothness of the weighting kernel, the phason field $\mathbf{h}(\mathbf{r})$, unlike the representative surface $\mathbf{f}(\mathbf{r})$, has derivatives that are continuous everywhere in parallel space [in general, the derivatives that appear in Eq. (5) are discontinuous at a tile edge].

The *phason strain* of an infinite square-triangle tiling, an $\mathbf{r}$-dependent perp.-space × parallel-space tensor, is defined as

$$\underline{E} = \begin{bmatrix} E_{11}, & E_{12} \\ E_{21}, & E_{22} \end{bmatrix} = \begin{bmatrix} \partial h_1/\partial r_1, & \partial h_1/\partial r_2 \\ \partial h_2/\partial r_1, & \partial h_2/\partial r_2 \end{bmatrix}; \tag{10}$$

its $\mathbf{r}$ dependence is implicit. Note that $\mathbf{h}(\mathbf{r}) = \text{const}$ or, equivalently, $\underline{E} = 0$ corresponds to 12-fold symmetry. Through Eq. (10) and the translational invariance of $\mathbf{r}'-\mathbf{r}$ (the argument of the weighting kernel), the irrotational property of square-triangle tilings (see Sec. II B) assumes the guise

$$E_{12} - E_{21} = 0. \tag{11}$$

B. Entropy density

Imagine the maximally random ensemble that comprises every infinite square-triangle tiling. This ensemble can be described by an *entropy density* [the ensemble is maximally random (the Hamiltonian is zero); the *free-energy density* divided by $-k_B T$ equals the entropy density] that depends only on the phason strain:

$$\sigma[\underline{E}] = s_a^r + \sum_{n=1}^{\infty} \sigma_n[\underline{E}]; \tag{12}$$

s_a^r is the entropy per unit area at zero phason strain; $\sigma_n[\underline{E}]$ denotes, collectively, every term that is nth order in the phason strain, i.e., nth order in E_{ij}.

Because the ensemble has 12-fold symmetry, the entropy density $\sigma[\underline{E}]$—hence each $\sigma_n[\underline{E}]$ that it contains—must be 12-fold symmetric. As a result, $\sigma_1[\underline{E}]$ must vanish; i.e., $\sigma[\underline{E}]$ must have a stationary point at $\underline{E} = 0$. Furthermore, the random-tiling hypothesis[28,2] demands that this stationary point be a maximum and that $\sigma_2[\underline{E}]$ not vanish. The approximation

$$\sigma[\underline{E}] \simeq s_a^r + \sigma_2[\underline{E}] + \sigma_3[\underline{E}] \tag{13}$$

is henceforth assumed, with no further theoretical justification. As derived in Appendix A, the general forms for $\sigma_2[\underline{E}]$ and $\sigma_3[\underline{E}]$ are

$$\sigma_2[\underline{E}] = -\tfrac{1}{2}K_\mu (E_{11} + E_{22})^2 - \tfrac{1}{2}K_\nu (E_{12} - E_{21})^2 - \tfrac{1}{2}K_\xi (E_{12}E_{21} - E_{11}E_{22}), \tag{14}$$

where K_μ, K_ν, and K_ξ are three second-order elastic constants; and

$$\sigma_3[\underline{E}] = -\tfrac{1}{6} J\,(E_{11} - E_{22})[(E_{11} - E_{22})^2 - 3(E_{12} + E_{21})^2], \tag{15}$$

where J is a (the one and only) third-order elastic constant. Equation (14) is equivalent to Eq. (53) of Socolar's paper.[24] By way of Eq. (11) (the irrotational property), the middle group on the right-hand side of Eq. (14) (viz., the terms whose common multiplier is K_ν) vanishes. The random-tiling hypothesis demands that $\sigma_2[\underline{E}]$ be negative semidefinite, which in turn demands that

$$K_\mu,\ K_\xi \geq 0 \tag{16}$$

and

$$4K_\mu - K_\xi \geq 0. \tag{17}$$

The latter inequality provides a nontrivial consistency check between estimates of K_μ and K_ξ (see Sec. VII F).

C. Background phason strain

An infinite square-triangle tiling that is *well-behaved*[29] has a *background phason strain*, an $\mathbf{r}$-independent perp.-space $\times$ parallel-space tensor, that is defined as

$$\underline{B} = \begin{bmatrix} B_{11}, & B_{12} \\ B_{21}, & B_{22} \end{bmatrix} = \lim_{\Lambda\to\infty} \int \underline{E}(\mathbf{r}')\, \mathcal{W}(\mathbf{r}' - \mathbf{r})\, d^2\mathbf{r}'; \tag{18}$$

if the infinite square-triangle tiling were not well behaved, the background phason strain $\underline{B}$ would be $\mathbf{r}$ dependent; i.e., the limit $\Lambda \to \infty$ would be ill defined. Now, imagine the maximally random *subensemble*[30] that comprises every infinite square-triangle tiling whose background phason strain $\underline{B}$ takes the form

$$\begin{aligned} B_{11} &= -B_{22} = B, \\ B_{12} &= B_{21} = 0, \end{aligned} \tag{19}$$

where B is a certain real number. Any subensemble of this type has fourfold symmetry; $[I, D]$-type unit cells (see Sec. V C) have background phason strains that take the above form. The subsequent analysis [viz., Eq. (22)] is applicable only to subensembles whose background phason strains are small; assume henceforth that $B \ll 1$.

The entropy density given by Eqs. (13)–(15) describes the maximally random ensemble that comprises every infinite square-triangle tiling. A *modified*[31] entropy density is needed to describe the above subensemble. Such an entropy density ($\omega[\underline{\tilde{E}}]$ below) can be derived from the (unmodified) entropy density $\sigma[\underline{E}]$ through a Legendre transformation:

$$\underline{\tilde{E}} = \underline{E} - \underline{B}, \tag{20}$$

$$\omega[\underline{\tilde{E}}] = \sigma[\underline{E}] - \sum_{i=1}^{2}\sum_{j=1}^{2} \lambda_{ij}\tilde{E}_{ij}; \tag{21}$$

$\underline{\tilde{E}}$ is the ($\mathbf{r}$-dependent) modified phason strain; the λ_{ij} are Lagrange multipliers, which are determined by demanding that $\omega[\underline{\tilde{E}}]$ be stationary at $\underline{\tilde{E}} = 0$. Note that, if $B = 0$, $\omega[\underline{\tilde{E}}] = \sigma[\underline{E}]$; that is, the Legendre transformation is the identity if the background phason strain $\underline{B}$ vanishes. (A thermodynamic limit is implicit: A subensemble that corresponds to $B \neq 0$ has a vanishing weight within the ensemble that comprises every infinite square-triangle tiling.) Assuming Eq. (19) and neglecting every term that is higher than second order in either $\tilde{E}_{ij}$ or B, the modified entropy density takes the form

$$\begin{aligned} \omega[\underline{\tilde{E}}] = [s_a^r - \tfrac{1}{2}K_\xi B^2] \\ -\tfrac{1}{2}K_\mu\,(\tilde{E}_{11} + \tilde{E}_{22})^2 \\ -\tfrac{1}{2}K_\xi\,(\tilde{E}_{12}\tilde{E}_{21} - \tilde{E}_{11}\tilde{E}_{22}) \\ -JB[(\tilde{E}_{11} - \tilde{E}_{22})^2 - (\tilde{E}_{12} + \tilde{E}_{21})^2]. \end{aligned} \tag{22}$$

Note that the last group on the right-hand side of Eq. (22)—hence $\omega[\underline{\tilde{E}}]$ itself—is only fourfold symmetric.[32] This makes sense: The subensemble that the modified entropy density $\omega[\underline{\tilde{E}}]$ describes has only fourfold symmetry.

D. Finite systems

Consider a finite unit cell $\mathcal{C}$ that certain square-triangle approximants tile and the pair of primitive (parallel-space) translation vectors $\{\mathbf{A}^u, \mathbf{A}^v\}$ that prescribe this unit cell. The background phason strain of the unit cell $\mathcal{C}$ is defined implicitly through

$$\underline{B}_c \cdot \mathbf{A}^u = \underline{B}_c \cdot \mathbf{A}^v = 0. \tag{23}$$

To avoid needless generalization, assume henceforth that the unit cell $\mathcal{C}$ is square, with a side length equal to L; $[I, D]$-type unit cells (see Sec. V C) are square.

Now consider a (any) square-triangle approximant that tiles the above unit cell $\mathcal{C}$. This approximant can be duplicated [that is, translated through all parallel-space vectors $\mathbf{G} = \sum_{ij} i\mathbf{A}^u + j\mathbf{A}^v$ (i and j are integers)] to form a continuous, infinite, yet periodic, square-triangle tiling; this (the latter) approximant is referred to as the *extended* square-triangle approximant in what follows. The modified perp.-space position vector of a vertex in the extended square-triangle approximant is defined as

$$\tilde{\mathbf{f}}_v = \mathbf{f}_v - \underline{B}_c \cdot \mathbf{r}_v, \tag{24}$$

where $\mathbf{f}_v$ is the (unmodified) perp.-space position vector of the vertex [see Eq. (4)], and $\mathbf{r}_v$ is the parallel-space position vector of the vertex [see Eq. (1)]. Similarly, the (infinite) modified representative surface of the extended square-triangle approximant is defined as

$$\tilde{\mathbf{f}}(\mathbf{r}) = \mathbf{f}(\mathbf{r}) - \underline{B}_c \cdot \mathbf{r}, \tag{25}$$

where $\mathbf{f}(\mathbf{r})$ is the (unmodified) representative surface of the extended square-triangle approximant. The modified phason field of the square-triangle approximant is defined [cf. Eq. (9)] as

$$\tilde{\mathbf{h}}(\mathbf{r}) = (\tilde{h_1}(\mathbf{r}), \tilde{h_2}(\mathbf{r}))^\perp = \int \tilde{\mathbf{f}}(\mathbf{r}')\, \mathcal{W}(\mathbf{r}' - \mathbf{r})\, d^2\mathbf{r}'. \tag{26}$$

Note that coarse graining requires that $1 \ll \Lambda \ll L$ and

thus fails for small side lengths L. The modified phason strain of the square-triangle approximant (i.e., $\underline{\tilde{E}}$, whose $\mathbf{r}$ dependence is implicit) is defined as

$$\tilde{E}_{ij} = \frac{\partial \tilde{h}_j}{\partial r_i}. \tag{27}$$

By construction, the modified phason field $\tilde{\mathbf{h}}(\mathbf{r})$ is periodic over the unit cell $\mathcal{C}$ and can thus be expressed as a Fourier series:

$$\tilde{\mathbf{h}}(\mathbf{r}) = \frac{1}{L}\sum_{\mathbf{k}} \tilde{\mathbf{h}}(\mathbf{k})\mathcal{V}(\mathbf{k})e^{-i\mathbf{k}\cdot\mathbf{r}}; \tag{28}$$

$\mathbf{k} = (k_1, k_2)^{\|}$ is a Fourier wave vector; the *phason modes* $\tilde{\mathbf{h}}(\mathbf{k})$ are defined as

$$\tilde{\mathbf{h}}(\mathbf{k}) = (\tilde{h_1}(\mathbf{k}), \tilde{h_2}(\mathbf{k}))^{\perp} = \frac{1}{L}\int_{\mathcal{C}} \tilde{\mathbf{f}}(\mathbf{r}')e^{i\mathbf{k}\cdot\mathbf{r}'}\, d^2\mathbf{r}'; \tag{29}$$

the *attenuation function* $\mathcal{V}(\mathbf{k})$ is related to the weighting kernel $\mathcal{W}(\mathbf{r})$ by

$$\mathcal{V}(\mathbf{k}) = \int \mathcal{W}(\mathbf{r}')e^{i\mathbf{k}\cdot\mathbf{r}'}\, d^2\mathbf{r}', \tag{30}$$

provided that $\mathcal{W}(\mathbf{r})$ is sensible (viz., smooth, normalized, and with a well-defined characteristic width Λ), $\mathcal{V}(\mathbf{k}) \approx 1$ for $|\mathbf{k}| \ll 2\pi/\Lambda$, but $|\mathcal{V}(\mathbf{k})| \ll 1$ for $|\mathbf{k}| \gg 2\pi/\Lambda$. Because $\underline{B}_c \cdot \mathbf{r}$ is irrotational, the irrotational property [see Eqs. (5) and (11)] holds for the modified phason field $\tilde{\mathbf{h}}(\mathbf{r})$ [note Eq. (27)]:

$$\tilde{E}_{12} - \tilde{E}_{21} = 0. \tag{31}$$

The modified phason field can be expressed as the gradient of a *(gauge-fixed and modified) scalar-potential field* [see Ref. 33; cf. Eq. (7)]:

$$\tilde{\mathbf{h}}(\mathbf{r}) = \nabla\tilde{\Psi}(\mathbf{r}). \tag{32}$$

Furthermore, the phason modes [Eq. (29)] can be related to *scalar-potential modes* (see Refs. 33 and 34):

$$\tilde{\mathbf{h}}(\mathbf{k}) = -i\mathbf{k}\tilde{\Psi}(\mathbf{k}). \tag{33}$$

E. Modified entropy functional

Every distinct approximant that tiles the (finite) unit cell $\mathcal{C}$ can be duplicated to form a unique extended approximant, whose background phason strain $\underline{B}$ [see Eq. (18)] equals $\underline{B}_c$. Most infinite square-triangle tilings whose background phason strains $\underline{B}$ equal $\underline{B}_c$, however, are not extended approximants; i.e., they are not capable of being collapsed (that is, "unduplicated") onto the unit cell $\mathcal{C}$. Assume, henceforth, that the background phason strain $\underline{B}_c$ takes the form of Eq. (19) [with $\underline{B} = \underline{B}_c$].

Imagine the maximally random *sub-subensemble*[30] comprising every square-triangle approximant that tiles the unit cell $\mathcal{C}$. The maximally random subensemble (see Sec. III C) that comprises every infinite square-triangle tiling whose background phason strain $\underline{B}$ equals $\underline{B}_c$ contains this sub-subensemble as a subset. In the thermodynamic limit $L \to \infty$, the subensemble and the sub-subensemble are equivalent. Thus, neglecting *finite-L effects*, the sub-subensemble can be described by a *modified entropy functional* that is defined as

$$\Omega = \int_{\mathcal{C}} \omega[\underline{\tilde{E}}(\mathbf{r})]\, d^2\mathbf{r}. \tag{34}$$

Using Eqs. (27) and (28), the modified entropy functional can be expressed as a function of the phason modes:

$$\begin{aligned}\Omega = {} & [s_a^r - \tfrac{1}{2}K_\xi B^2]\mathcal{A} \\ & -\tfrac{1}{2}\sum_{\mathbf{k}} \mathcal{V}(\mathbf{k}) \Big\{ K_\mu |k_1\tilde{h}_1[\mathbf{k}] + k_2\tilde{h}_2[\mathbf{k}]|^2 \\ & \qquad +2JB[|k_1\tilde{h}_1[\mathbf{k}] - k_2\tilde{h}_2[\mathbf{k}]|^2 \\ & \qquad -|k_2\tilde{h}_1[\mathbf{k}] + k_1\tilde{h}_2[\mathbf{k}]|^2] \Big\}. \end{aligned} \tag{35}$$

As Socolar notes,[24] the third group on the right-hand side of Eq. (22) (viz., the terms whose common multiplier is K_ξ) is a total divergence and thus vanishes for any modified phason field $\tilde{\mathbf{h}}(\mathbf{r})$, which, by definition, is periodic over the region of integration ($\int_{\mathcal{C}} d^2\mathbf{r}$). Using Eq. (33), the modified entropy functional Ω [Eq. (35)] can be reexpressed as a function of the modified scalar-potential modes:

$$\begin{aligned}\Omega = {} & [s_a^r - \tfrac{1}{2}K_\xi B^2]\mathcal{A} \\ & -\tfrac{1}{2}\sum_{\mathbf{k}} \mathcal{V}(\mathbf{k}) \{K_\mu + 2JB\cos(4\theta_{\mathbf{k}})\} |\mathbf{k}|^4 |\tilde{\Psi}(\mathbf{k})|^2, \end{aligned} \tag{36}$$

where $\theta_{\mathbf{k}} = \tan^{-1}(k_1/k_2)$. Equation (36) is the jewel of the continuum theory and the hub of this paper. Note that its (relative) simplicity stems from the irrotational property of square-triangle tilings (Sec. II B) and from the special (symmetric) form [Eq. (19)] that the background phason strain $\underline{B}$ takes.

F. Fluctuations

The modified scalar-potential modes $\tilde{\Psi}(\mathbf{k})$ that appear in Eq. (36) compose a set of complex variables that parametrize (note Ref. 34) the sub-subensemble. These variables are independent except for the relations $\tilde{\Psi}(-\mathbf{k}) = \tilde{\Psi}^*(\mathbf{k})$, which ensure that the modified phason field $\tilde{\mathbf{h}}(\mathbf{r})$ is real valued. Consider expectations of the form $\langle \tilde{h}_i(\mathbf{k})\tilde{h}_j^*(\mathbf{k})\rangle$, where $i, j \in \{1, 2\}$. Using Eq. (33),

$$\langle \tilde{h}_i(\mathbf{k})\tilde{h}_j^*(\mathbf{k})\rangle = k_i k_j \langle \tilde{\Psi}(\mathbf{k})\tilde{\Psi}^*(\mathbf{k})\rangle. \tag{37}$$

Assume henceforth that $\mathbf{k} \ll 2\pi/\Lambda$, i.e., that (in effect) $\mathcal{V}(\mathbf{k}) = 1$. Using Eq. (36),

$$\langle \tilde{h}_i(\mathbf{k})\tilde{h}_j^*(\mathbf{k})\rangle = \frac{k_i k_j}{\{K_\mu + 2JB\cos(4\theta_{\mathbf{k}})\}|\mathbf{k}|^4}. \tag{38}$$

Thus, the values of K_μ and J can be deduced from the magnitude of $\langle \tilde{h}_i(\mathbf{k})\tilde{h}_j^*(\mathbf{k})\rangle$ at different values of B and $\mathbf{k}$. The rest of this paper deals almost exclusively with sub-subensembles comprising random square-triangle approximants. To avoid what might, by some, be mistaken for pedantry, a "sub-subensemble" is called an ensemble, henceforth.

IV. UPDATE MOVE: CONNECTIVITY AND ZIPPERS

This section motivates, defines, and discusses an update move, which the Monte Carlo runs that are described in this paper (Secs. VI E, VI B, VI E, and VII E and Appendix C) used. Some overlap exists between what follows and the discussion apropos "ergodicity" in Henley's review article.[35]

An update move *connects* two objects if either object can be obtained from the other by applying the update move one or more times. Extending this definition, an update move *connects* an ensemble (comprising "objects") if every member of the ensemble can be obtained from every other member of the ensemble by applying the update move one or more times. An update move is *adequate* for an ensemble if it connects the ensemble. To sample an ensemble representatively, a Monte Carlo *step*[36] requires an update move that is adequate for the ensemble.

The objects with which this paper is concerned are (random square-triangle) tilings. An update move exists that connects random rhombus tilings, which rotates the 3 tiles inside a hexagon by 180°.[28,37] The analogous update move for square-triangle tilings rotates the 18 tiles (6 squares and 12 triangles) inside a dodecagon by 30°. This (the latter) update move, however, is *inadequate*; it does not connect arbitrary (random) square-triangle tilings.[38] To sample ensembles of random square-triangle tilings representatively, more complex rearrangements of squares and triangles need to be considered. Such rearrangements are *zippers*; this word (in the singular) is defined in Sec. I, third paragraph. Look at Fig. 3. Every Monte Carlo run that is described in this paper (Secs. VI B, VI E, and VII E and Appendix C) used an update move that effects a zipper. The precise formulation of this update move is as follows.

(i) First, a region that comprises an adjoining square and triangle is selected at random, then repartitioned to form a pair of thin rhombi and a triangle. Each thin rhombus is given a *sense of direction* that points away from the other, which is represented by an arrow between its (the rhombus') two obtuse corners. See Fig. 4(a).

(ii) Next, the two thin rhombi execute *submoves* alternately [one of the rhombi is picked at random ("50-50") to be the rhombus that executes the first submove], where a submove is either an "A-type flip," a "B-type flip," or a "bounce." See Figs. 4(b)–4(d). Note that an A-type or B-type flip entails a rearrangement of only those tiles that lie around a single vertex; these tiles cover a region whose exterior remains unaltered by the flip. When a rhombus executes a B-type flip, one of the two rearrangements that are possible is chosen at random (50-50). A bounce merely reverses a rhombus' sense of direction.

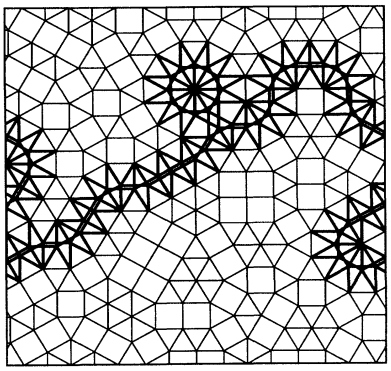

FIG. 3. Square-triangle tiling (a non-Stampfli [2, 1]-type square-triangle approximant (see Sec. V C)) both before and after a simple realization of the zipper update move. The tile edges that do not occur both before and after are drawn more boldly so as to highlight the zipper. The reader should note that a typical realization effects a zipper that is both longer and more complex [as regards self-intersections and homology (viz., *winding numbers*—the boundary conditions of an approximant are toroidal)] than the zipper shown.

(iii) If, after the execution of a submove, the two thin rhombi and a triangle compose a region whose shape is the same as a region that comprises an adjoining square and triangle, the region is repartitioned into such a square and triangle, thereby terminating the update move. See Fig. 4(e).

To recast (i)–(iii) in less precise though more romantic language: A pair of thin rhombi are first created; each rhombus then meanders independently through the square-triangle tiling, in a way vaguely analogous to the operation of a zip fastener. The two rhombi sometimes scatter off one another, but sooner or later they mutually annihilate; they leave as their lives' work a zipper of squares and triangles.

Throughout this paper, the above update move is called the *zipper update move*. Because it requires only local manipulations, the zipper update move can be implemented on a computer without too much difficulty. Note that the above prescription only works if the square-triangle tiling in which the zipper update move is executed has no boundaries. In practice, the zipper update move is applied only to finite square-triangle approximants, which by definition (Sec. I, second paragraph) satisfy periodic (toroidal) boundary conditions and thus have no boundaries. Section VI B considers how the mean (average) length of a zipper scales with unit-cell size. Note that B-type flips involve random choices; a zipper of squares and triangles is a random walk. Because the trail left by a thin rhombus is defect free, a zipper can cross over the same squares and triangles more than once; its random walk can self-intersect.

But is the zipper update move adequate? That is, does it connect (arbitrary) random square-triangle

tilings? The authors reckon that Levitov has discovered the basis of a proof.[39] A diagnostic quantity as regards this question is s_v^r, the entropy per vertex of (infinite) random square-triangle tilings at zero phason strain. Kawamura[40] obtained an estimate of s_v^r using a numerical transfer-matrix method; Widom[41,42] recently obtained an amazingly accurate estimate of s_v^r using a numerical Bethe-ansatz–transfer-matrix method. By way of Monte Carlo runs (Sec. VII E), the authors obtained (Sec. VII F) an estimate of s_v^r [Eq. (93)] that equals, within random-systematic errors, Kawamura's and Widom's (independent) estimates. This suggests that the zipper update move connects as many square-triangle tilings as Kawamura's and Widom's transfer matrices generate. Hence, the authors believe that the zipper update move is indeed adequate for ensembles that comprise random square-triangle tilings.

Though motivated more by necessity than by a need for computational efficiency, the zipper update move resembles, somewhat, the "cluster-flip" processes that underlie the Swendsen-Wang[44] and Wolff[45] algorithms. Both the *athermal Monte Carlo step* (see Sec. VI A) and the *thermal*[46] *Monte Carlo step* (see Sec. VII D) incorporate the zipper update move. The dynamics of the athermal Monte Carlo step, as regards the mean length of a zipper and the autocorrelation times of phason modes, is considered in Secs. VI B, VI D, and VI F.

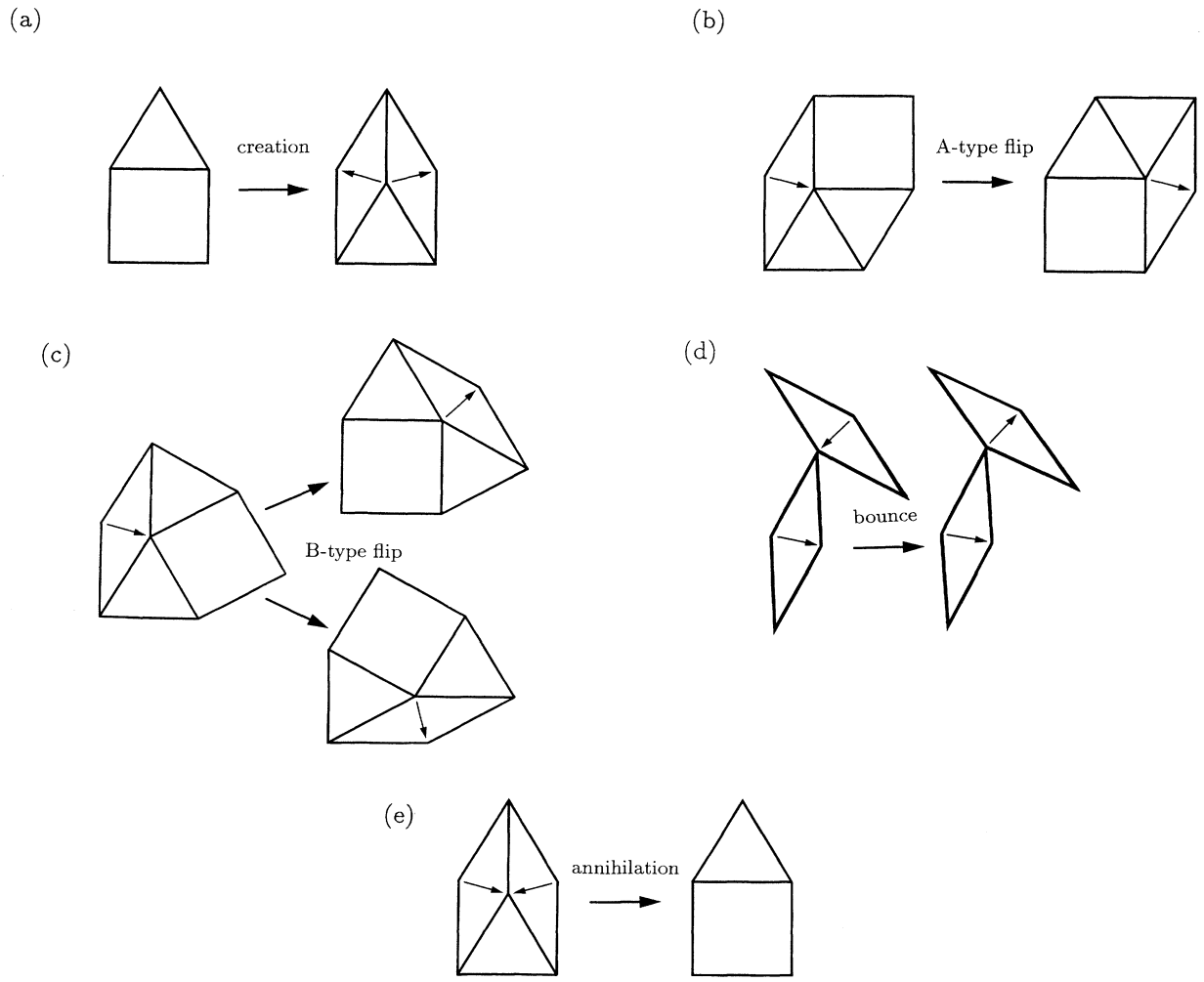

FIG. 4. Details of the zipper update move: (a) the creation of a pair of thin rhombi; (b) an A-type flip (one of two); the other A-type flip (not shown) is related to the A-type flip that is shown by (i) a reflection of the "before" arrangement, through the line that joins the obtuse corners of the thin rhombus that the before arrangement contains then (ii) a reflection of the "after" arrangement, through the line that joins the obtuse corners of the thin rhombus that the after arrangement contains; (c) the B-type flip; (d) a (generic) bounce (one of six); the other five bounces are not shown; two of the other five bounces are related to the bounce that is shown through a rotation of the "active" thin rhombus, whose arrow reverses direction, by $\pi/3$ radians clockwise and $\pi/6$ radians anticlockwise, respectively, about the point at which the two thin rhombi touch; these two bounces and the bounce that is shown are related to the other three bounces by a reflection of both the before and after arrangements, through the line that joins the obtuse corners of the "passive" thin rhombus, whose arrow does not reverse direction; (e) the annihilation of a pair of thin rhombi.

V. STAMPFLI TILINGS

To motivate what follows, several observations—unequal with respect to their acuity, yet equal with respect to their significance—are made: (i) Monte Carlo simulations run on computers; (ii) every such machine has only a finite amount of memory and runs at only a finite speed; (iii) a tiling that tiles a unit cell whose extent is finite (i.e., a *finite* approximant), unlike a quasiperiodic (infinite) tiling, can be represented in a finite amount of computer memory; (iv) a Monte Carlo run requires a *starting configuration*; (v) a system without boundaries cannot suffer from surface (finite-size) effects;[47] (vi) an approximant defines a system without boundaries; that is (note Ref. 5), it (the approximant) engenders an ensemble that comprises every approximant that tiles the same unit cell as it (the approximant) tiles; (vii) an approximant can serve as the starting configuration of a Monte Carlo run that samples the ensemble that it (the approximant) engenders; (viii) the amount of (real) computer time that is needed to execute the number of Monte Carlo steps that are sufficient to *decorrelate* a system increases with the size of the system; (ix) accurate estimates of a system's elastic constants and/or its entropy per unit area at zero phason strain require Monte Carlo runs that sample ensembles that correspond to small background phason strains.

The above observations call for the construction of finite square-triangle approximants whose background phason strains are small. Section V A defines an inflation rule (viz., the random-Stampfli inflation rule), whereby such approximants can be built. This inflation rule contains random choices; as a result, it engenders a nonzero entropy per vertex. Section V B explains how, via recursion, the value of this entropy per vertex at 12-fold symmetry (i.e., zero phason strain) can be computed. Section V C describes the (random-Stampfli) square-triangle approximants that served as the starting configurations of Monte Carlo runs (Secs. VI B, VI E, and VII E and Appendix C), and presents formulas for quantities that depend only on the periodic boundary conditions that such approximants satisfy.

A. Random-Stampfli inflation

Stampfli discovered an inflation rule for square-triangle tilings.[19] The authors used the maximally random version of this rule,[48] whose definition can be broken down into four parts.

(RS 1) First, scale up the *parent* square-triangle tiling that already exists by a factor of λ (the inflation constant) $\equiv (2+\sqrt{3})$. (The analog of λ for tenfold-symmetric rhombus tilings is the golden ratio.)

(RS 2) Next, place regular (unit side length) dodecagons on the *big* parent square-triangle tiling, with their centers lying at vertices and their sides running perpendicular to tile edges; then erase the big parent square-triangle tiling.

(RS 3) Next, tile each dodecagon with 6 squares and 12 triangles in one of the two distinct ways that are possible; choose it (the way that is chosen) at random (50-50). [Either way corresponds to the same (sixfold-symmetric) pattern, but at a different orientation; the two orientations differ by 30°.]

(RS 4) Finally, tile the gaps that exist between the dodecagons; fill in the gap that exists between every three dodecagons, whose centers lie at the vertices of a big triangle, with a single triangle; fill in the gap that exists between every four dodecagons, whose centers lie at the vertices of a big square, with four triangles and a square. An *offspring* square-triangle tiling is thus created.

Figure 5 illustrates this, the *random-Stampfli*, inflation rule. The (random-)Stampfli inflation rule generates *Stampfli* (square-triangle) tilings.

B. Random-Stampfli entropy via recursion

Imagine the maximally random ensemble comprising every distinct Stampfli tiling that can be grown from a certain *seed* (viz., a small, hand-built square-triangle tiling) by applying the above inflation rule I times; $\mathcal{N}_S(I)$ Stampfli tilings compose the ensemble; each contains $N_v(I)$ vertices. The quantities $\mathcal{N}_S(I)$ and $N_v(I)$ are related by

$$\mathcal{N}_S(I) = \prod_{I'=0}^{I-1} 2^{N_v(I')}. \tag{39}$$

The entropy per vertex of the ensemble is

$$\frac{\ln[\mathcal{N}_S(I)]}{N_v(I)} = \ln[2] \sum_{I'=0}^{I-1} \frac{N_v(I')}{N_v(I)}. \tag{40}$$

The inflation constant of the Stampfli inflation rule equals λ; thus

$$\lim_{I'\to\infty} \frac{N_v(I'+1)}{N_v(I')} = \lambda^2. \tag{41}$$

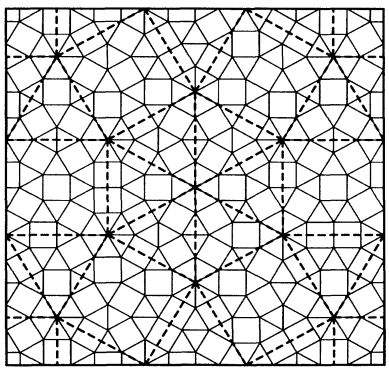

FIG. 5. Random-Stampfli inflation: a big parent square-triangle tiling (thick, dashed lines) and an offspring square-triangle tiling (thin, solid lines); both are periodic over the same, square unit cell (thick, solid lines).

Now consider the limiting entropy per vertex defined as

$$s_v^S = \lim_{I\to\infty} \frac{\ln[\mathcal{N}_S(I)]}{N_v(I)}. \quad (42)$$

This quantity is independent of the seed upon which the ensemble is rooted. Using Eqs. (40)–(42),

$$s_v^S = \ln[2] \sum_{I'=0}^{\infty} \frac{1}{\lambda^{2(I'+1)}} = \frac{\ln[2]}{[\lambda^2-1]} \approx 0.053615. \quad (43)$$

(This result appears in Appendix A of Ref. 23.) As $I \to \infty$, the number of vertices per unit area tends to $(\frac{1}{2}+\frac{1}{\sqrt{3}})$ [see Sec. V C, Eqs. (48)–(50)]. The entropy per unit area in the limit $I \to \infty$ is thus

$$s_a^S = s_v^S(\tfrac{1}{2}+\tfrac{1}{\sqrt{3}}) = \ln[2]/12 \approx 0.057762. \quad (44)$$

Sections VII and VIII and Appendix C all concern methods for estimating s_v^r or, equivalently, s_a^r; these two quantities are the analogs of s_v^S and s_a^S, respectively, for the maximally random ensemble of all infinite square-triangle tilings (not just infinite Stampfli tilings) at zero (background) phason strain. Because this ensemble contains every infinite Stampfli tiling (see Ref. 50), s_v^S and s_a^S contribute to s_v^r and s_a^r.

C. $[I, D]$-type square-triangle approximants

Consider a $D \times D$ array of squares that tiles a unit cell of side length D. Now imagine a square-triangle approximant that is grown from this array by applying the random-Stampfli inflation rule I times. Henceforth, label as "$[I, D]$-type" both the (square) unit cell that such a Stampfli approximant tiles and any (random) square-triangle approximant (either Stampfli or non-Stampfli[50]) that tiles the same unit cell. The side length of an $[I, D]$-type unit cell is

$$L = D\lambda^I, \quad (45)$$

where $\lambda \equiv (2+\sqrt{3})$ is the inflation constant [see Sec. V A, part (RS 1)]. The Fourier wave vectors for $[I, D]$-type unit cells are

$$\mathbf{k} = (2\pi/L)\ (p_1, p_2)^{\|}, \quad (46)$$

where p_1 and p_2 are integers. The background phason strain of an $[I, D]$-type unit cell takes the (diagonal) form of Eq. (19) [with $\underline{B} = \underline{B}_c$], where

$$B = \lambda^{-2I}. \quad (47)$$

Note that B depends only on the inflation order I and that B vanishes as $I \to \infty$. An $[I, D]$-type square-triangle approximant contains N_s squares, N_t triangles, and N_v vertices, where

$$\begin{bmatrix} N_s \\ N_t \end{bmatrix} = \begin{bmatrix} 7 & 3 \\ 16 & 7 \end{bmatrix}^I \begin{bmatrix} D^2 \\ 0 \end{bmatrix} \quad (48)$$

and

$$N_v = N_s + \tfrac{1}{2}N_t. \quad (49)$$

The (integer) components of the above matrix [Eq. (48)] can be deduced by counting squares and triangles from parts (RS 3) and (RS 4) of the random-Stampfli inflation rule (Sec. V A). As the inflation order $I \to \infty$ (i.e., in the limit of 12-fold symmetry), the number of vertices per unit area becomes

$$v_a = (\tfrac{1}{2}+\tfrac{1}{\sqrt{3}}) \approx 1.07735; \quad (50)$$

this quantity can be computed from the eigenvector that corresponds to the largest eigenvalue of the above matrix [Eq. (48)]. Now, the total entropy of the maximally random ensemble that, for a given $[I, D]$, comprises all $[I, D]$-type Stampfli approximants is

$$S^S[I, D] = \ln[\mathcal{N}_S(I, D)] = \ln[2] \sum_{I'=0}^{I-1} N_v(I', D), \quad (51)$$

where $N_v(I, D)$ is the (common) number of vertices that each $[I, D]$-type approximant contains [see Eqs. (48) and (49) above].

VI. PHASON FLUCTUATIONS VIA MONTE CARLO SIMULATIONS

This section describes how the authors obtained estimates of phason-mode fluctuations. Such quantities are related to the expectation that appears on the left-hand side of Eq. (38) and thus to the values of the elastic constants (K_μ and J) that appear in the denominator on the right-hand side of the same equation. Though directed towards random square-triangle tilings, many of the remarks that are made below are general. The details should be of service to a reader who is setting up Monte Carlo simulations to study either systems that involve random tilings or spin systems with height representations.

A. Athermal Monte Carlo step

The *athermal Monte Carlo step* used by athermal Monte Carlo runs (Sec. VI E) is defined as follows.

(i) From the *original* square-triangle tiling that already exists, a *trial* square-triangle tiling is generated by applying the zipper update move (Sec. IV).

(ii) The value of N_h' is determined; then the ratio

$$C = \frac{N_h}{N_h'} \quad (52)$$

is calculated; N_h (whose value is assumed to be already known from the previous athermal Monte Carlo step) and N_h' are the numbers of regions that comprise an adjoining square and triangle in the original and trial tilings, respectively.

(iii) If $C \geq 1$, the trial tiling is *accepted* (i.e., it is

maintained in the memory of the computer). If $C < 1$, a pseudorandom number R between 0 and 1 is calculated; the trial tiling is accepted if $R < C$; else it is *rejected* (i.e., it is erased from the memory of the computer).

The athermal Monte Carlo step satisfies *detailed balance*, and as a result, a maximally random ensemble of square-triangle tilings is *stationary* under it (see Refs. 51 and 52). A proof of detailed balance is given in Appendix B. At least for random square-triangle tilings (approximants) that are large, the value of C is typically close to 1, and the trial square-triangle tiling is, as a result, almost always accepted. Unlike Monte Carlo steps that contain *flip* update moves,[8–10,37,74] the above Monte Carlo step rearranges (on average) a huge number of tiles. On a technical note, the amount of computer time that is needed to determine the number of regions that comprise an adjoining square and triangle in an approximant (i.e., the value of N_h or N'_h) scales proportionally to the area of the unit cell (the area of an $[I, D]$-type unit cell is $L^2 = D^2\lambda^{2I}$).

B. Athermal zipper length

How does the mean (average) length of a zipper scale with unit-cell size? An answer to this question first requires a—natural yet unambiguous—definition of a zipper's length. Because thin rhombi can bounce [see Fig. 4(d)] and because a zipper can cross over the same squares and triangles more than once, several different (though perhaps equally appealing) definitions are conceivable. The length L_Z of a zipper, by the authors' definition, is equal to $(1 + N_A + N_B)$, where N_A and N_B are the number of A-type flips and the number of B-type flips, respectively, that a zipper involves; in less precise though more intuitive language, L_Z equals the number of tile edges that run along the zipper's backbone. Henceforth, the *zipper length* of a Monte Carlo step denotes the length of the zipper that the step's zipper update move effects, irrespective of whether the zipper is accepted or rejected. The lowest possible value of L_Z is 6, which corresponds to the rotation of a dodecagon by 30° [i.e., the update move that is inadequate for random square-triangle tilings—see Sec. IV and Ref. 38; cf. Sec. V A, parts (RS 2) and (RS 3)]. The amount of computer time needed to effect a zipper scales proportionally to L_Z.

Stampfli $[1, D]$-type approximants for $D = 2, 3, \ldots, 16$ were built. To each approximant, 10^4 athermal Monte Carlo steps were first applied (an equilibration stage—see Sec. VI D); then a further 10^5 athermal Monte Carlo steps were applied (a measurement stage). The zipper lengths of the steps in each measurement stage were calculated, by counting A-type and B-type flips, then *binned* to form a histogram. Above the lower cutoff at $L_Z = 6$, each histogram (for $D \geq 4$ at least) took the shape of a Poisson distribution. An estimate of the mean zipper length $\langle L_Z \rangle$ was calculated for each D; see Fig. 6. A naive argument,[53] based on the idea of an annihilation cross section, would predict that $\langle L_Z \rangle$ scales proportionally to $L^2 \propto D^2$. Figure 6 seems to support this scaling relationship, though the possibility of logarithmic corrections (as occur with random walks in two dimensions) cannot be ruled out.

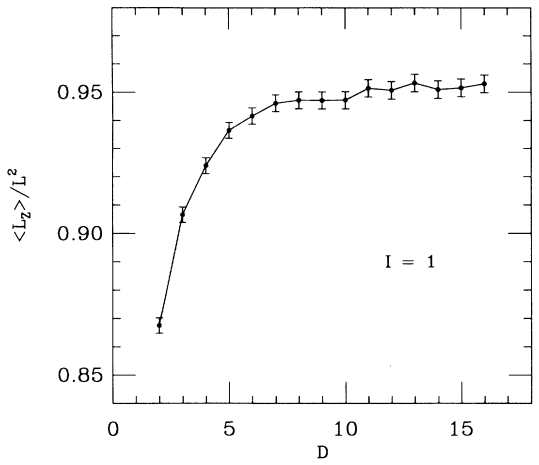

FIG. 6. Zipper-length scaling: Estimates of mean zipper length $\langle L_Z \rangle$ divided by unit-cell area L^2, against array dimension D. The random error of each estimate assumes Poisson statistics.

C. Phason-mode fluctuations

Imagine a maximally random ensemble of $[I, D]$-type square-triangle approximants (each member of the ensemble tiles the same $[I, D]$-type unit cell). Consider an expectation of the form $\langle \tilde{h}_i(\mathbf{k})\tilde{h}_i^*(\mathbf{k}) \rangle$ over this ensemble, where $i \in \{1, 2\}$ and the wave vector $\mathbf{k}$ is given by Eq. (46). An estimate of this expectation can be obtained by averaging the quantity $\tilde{h}_i(\mathbf{k})\tilde{h}_i^*(\mathbf{k})$ over a large, representative sample of the ensemble. Such a sample can be generated by executing the athermal Monte Carlo step (Sec. VI A) on a computer.

At this point, a few facts need stating.

(i) The amount of computer time needed to decorrelate a system [viz., to execute M zipper update moves; see Sec. VI E, stage (LAMC 2)] is always much greater than the amount of computer time needed to calculate a phason-mode component [i.e., an $\tilde{h}_i(\mathbf{k})$].

(ii) A maximally random ensemble of $[I, D]$-type approximants has fourfold symmetry; expectations of the form $\langle \tilde{h}_i(\mathbf{k})\tilde{h}_i^*(\mathbf{k}) \rangle$ over such an ensemble are thus fourfold symmetric.

(iii) For any $[I, D]$-type approximant, the quantity $\tilde{h}_i(\mathbf{k})\tilde{h}_i^*(\mathbf{k})$ is invariant under reflections through Cartesian axes.

(iv) By way of Eq. (33), $k_1\tilde{h}_2(\mathbf{k}) = k_2\tilde{h}_1(\mathbf{k})$; see Ref. 34.

Consider *symmetry-averaged phason-mode intensities* defined, for $[I, D]$-type square-triangle approximants, as

$$\{|\tilde{h}_i(\mathbf{k})|^2\}' = \tfrac{1}{2}[|\tilde{h}_i(\mathbf{k})|^2 + |\tilde{h}_{i'}(\mathbf{k}')|^2], \tag{53}$$

where $i' = 1(2)$, if $i = 2(1)$, and $\mathbf{k}' = (k_2, k_1)^{\parallel}$, with $\mathbf{k} = (k_1, k_2)^{\parallel}$. Next, consider *symmetry-averaged phason-*

mode fluctuations defined, for maximally random ensembles of $[I,D]$-type square-triangle approximants, as

$$F_{(p_1,p_2)} = \langle \{ |\tilde{h}_i(\mathbf{k})|^2 \}' \rangle, \tag{54}$$

where the subscript (p_1,p_2), which acts as a label, corresponds, via Eq. (46), to the value of the wave vector $\mathbf{k}$ for $i = 1$. In view of facts (i)–(iv) above, the need for computational efficiency demands that long athermal Monte Carlo runs (see Sec. VI E) calculate symmetry-averaged phason-mode intensities $\{|\tilde{h}_i(\mathbf{k})|^2\}'$ and thereby estimate symmetry-averaged phason-mode fluctuations $F_{(p_1,p_2)}$; see Ref. 54; as regards computer time, this practice brings about a factor of 2 benefit. Next, consider *reduced symmetry-averaged phason-mode fluctuations* defined as

$$F_{(p_1,p_2)}|_{\mathrm{red}} = \left\{ \frac{4\pi^2(p_1^2+p_2^2)^2}{L^2 p_1^2} \right\} F_{(p_1,p_2)}. \tag{55}$$

The continuum theory [i.e., Sec. III, viz., Eq. (38)] predicts that

$$F_{(p_1,p_2)}|_{\mathrm{red}} = \frac{1}{K_\mu + 2JB\cos(4\theta_{\mathbf{k}})}. \tag{56}$$

Concerning the task of calculating phason-mode components $\tilde{h}_i(\mathbf{k})$, for which $|\mathbf{k}| \ll 1$, Eq. (29) can be replaced by the approximation

$$\tilde{\mathbf{h}}(\mathbf{k}) \simeq \frac{1}{L} \sum_{n=1}^{N_v} w(v_n) \tilde{\mathbf{h}}_{v_n} \exp[i\mathbf{k}\cdot\mathbf{r}_{v_n}], \tag{57}$$

where v_n is the nth vertex of the $[I,D]$-type square-triangle approximant, $w(v_n)$ is the *weight* of the nth vertex, and N_v is the number of vertices that the approximant contains; remember that $\tilde{\mathbf{h}}(\mathbf{k}) = (\tilde{h}_1(\mathbf{k}), \tilde{h}_2(\mathbf{k}))^\perp$. The weight of a vertex equals the area of its Voronoi region: $w(v_n) = 1$, $(2+\sqrt{3})/4$, $\sqrt{3}/2$ for a vertex v_n with four, five, or six nearest neighbors, respectively. In athermal Monte Carlo runs (Sec. VI E), phason-mode components $\tilde{h}_i(\mathbf{k})$ are calculated using Eq. (57).

D. Phason-mode autocorrelation functions

The questions whether or not a Monte Carlo run achieves *equilibration* and whether or not a Monte Carlo run effects *independent sampling* are both undecidable without knowledge of the relevant autocorrelation function(s). Consider a best value (a Monte Carlo time average) $\langle q \rangle_{\mathrm{BV}}$ for the expectation (the ensemble average) $\langle q \rangle$ of a (real-valued) quantity q. The random error $\langle q \rangle_{\mathrm{RE}}$ of this best value depends on the autocorrelation function $\langle q(0)q(\tau) \rangle$, where τ is the Monte Carlo time displacement. The characteristic (Monte Carlo) time τ^{corr} of an autocorrelation function that decays exponentially specifies the autocorrelation function completely. If the autocorrelation function $\langle q(0)q(\tau) \rangle$ decays exponentially and if a *rough*[55] best value for its characteristic time τ_q^{corr} is obtainable, a Monte Carlo run can then be set up, for which the best value $\langle q \rangle_{\mathrm{BV}}$ is free of systematic error (that is, equilibration is assured; viz., the equilibration stage of the Monte Carlo run contains sufficient Monte Carlo steps; see Ref. 56) and for which the random error $\langle q \rangle_{\mathrm{RE}}$ is both calculable and credible. A summary of this paragraph: autocorrelation functions are the difference between hope and belief.

Consider *symmetry-averaged phason-mode autocorrelation functions* that are defined, for maximally random ensembles of $[I,D]$-type square-triangle approximants, as

$$C_{(p_1,p_2)}[\tau] = \langle \tfrac{1}{2} [\tilde{h}_i(\mathbf{k};\tau)\tilde{h}_i^*(\mathbf{k};0) + \tilde{h}_{i'}(\mathbf{k}';\tau)\tilde{h}_{i'}^*(\mathbf{k}';0)] \rangle, \tag{58}$$

where the unit of Monte Carlo time (displacement) τ is an athermal Monte Carlo step and the subscript (p_1,p_2) corresponds [via Eq. (46)] to the value of the wave vector $\mathbf{k}$ for $i = 1$; $i' = 1(2)$, if $i = 2(1)$, and $\mathbf{k}' = (k_2,k_1)^\parallel$, with $\mathbf{k} = (k_1,k_2)^\parallel$. Note that $C_{(p_1,p_2)}[0] = F_{(p_1,p_2)}$ [see Eqs. (53) and (54)].

If both $|\mathbf{k}| \ll 1$ and $\tau_{(p_1,p_2)}^{\mathrm{corr}} \gg 1$ [see Eqs. (60) and (61) below], that is, if a *linear-response–hydrodynamic* description is applicable (see Ref. 9), the (athermal) Monte Carlo dynamics of a scalar-potential mode $\tilde{\Psi}(\mathbf{k})$ ought to obey

$$\frac{d\tilde{\Psi}(\mathbf{k};\tau)}{d\tau} = \Gamma \frac{\partial \Omega}{\partial \tilde{\Psi}(\mathbf{k})} + \zeta(\tau), \tag{59}$$

where Γ is a ($\mathbf{k}$-independent) rate constant, Ω is the entropy functional [see Eq. (36)], and $\zeta(\tau)$ is a noise term that satisfies $\langle \zeta(\tau'')\zeta(\tau') \rangle = 2\Gamma\delta(\tau''-\tau')$. [Equation (59) is a Langevin equation; it is the equivalent of Eq. (20) in Ref. 9, for "$\mathbf{p} \to 0$."] By way of Eqs. (33), (38), (53), (54), (58), and (59),[57]

$$C_{(p_1,p_2)}[\tau] = F_{(p_1,p_2)} \exp[\tau/\tau_{(p_1,p_2)}^{\mathrm{corr}}], \tag{60}$$

where

$$\tau_{(p_1,p_2)}^{\mathrm{corr}} = 1/[\Gamma\{K_\mu + 2JB\cos(4\theta_{\mathbf{k}})\}\,|\mathbf{k}|^2]. \tag{61}$$

[Equations (60) and (61) represent a special case of the fluctuation-dissipation theorem.]

E. Athermal Monte Carlo runs

Two distinct types of *athermal Monte Carlo run* were performed: *short* athermal Monte Carlo runs for estimating symmetry-averaged phason-mode autocorrelation functions $C_{(p_1,p_2)}[\tau]$, hence autocorrelation times $\tau_{(p_1,p_2)}^{\mathrm{corr}}$; *long* athermal Monte Carlo runs for estimating symmetry-averaged phason-mode fluctuations $F_{(p_1,p_2)}$, hence the second-order elastic constant K_μ and the third-order elastic constant J. Both short and long athermal Monte Carlo runs use the athermal Monte Carlo step (Sec. VI A). The setting up of each long athermal Monte Carlo run requires a short athermal Monte Carlo run: The value of M [see stage (LAMC 2) below] depends on the value of $\tau_{\mathrm{max}}^{\mathrm{corr}}$ [see stage (SAMC 4) below].

A short athermal Monte Carlo (SAMC) run comprises

four stages.

(SAMC 1) First, an $[I,D]$-type Stampfli approximant (see Sec. V C) is constructed using the random-Stampfli inflation rule (see Sec. V A). (A *binary-tree* sort[58] removes the duplicate vertices that arise where dodecagons touch. In constructing the requisite vertex-connectivity information, advantage is taken of the hierarchical relationships that exist between the vertices of Stampfli tilings: A vertex only searches among its *siblings* and *cousins* to discover the vertices to which it is connected by a tile edge.) Note that the inflation constant I and array dimension D specify the $[I,D]$-type unit cell that the Stampfli approximant tiles and hence the maximally random ensemble of $[I,D]$-type square-triangle approximants that the Monte Carlo run samples.

(SAMC 2) Next, the athermal Monte Carlo step (Sec. VI A) is applied E times [$E \gg \tau_{\max}^{\mathrm{corr}}$; a best value for $\tau_{\max}^{\mathrm{corr}}$ is calculated in stage (SAMC 4); see Ref. 59]. This stage equilibrates the Stampfli approximant generated in stage (SAMC 1).

(SAMC 3) Next, the athermal Monte Carlo step is applied G times. After each step, the values of certain phason-mode components $\tilde{h}_i(\mathbf{k})$ [viz., the $\tilde{h}_i(\mathbf{k})$ that are requisite for estimating the symmetry-averaged phason-mode autocorrelation functions $C_{(p_1,p_2)}[\tau]$, for $(p_1,p_2) = (1,0)$, $(1,1)$, $(2,0)$, $(2,1)$, $(3,0)$, and $(1,2)$] are calculated for the extant approximant, then stored in a memory loop (viz., a *linked list*[58] that bites its tail) that holds the values of these phason-mode components for the H most recent approximants. The contents of the memory loop are used to calculate best values for symmetry-averaged phason-mode autocorrelation functions $C_{(p_1,p_2)}[\tau]$ (see Sec. VI D), at Monte Carlo time displacements $\tau = 0, 1, \ldots, (H-1)$.

(SAMC 4) Finally, a best value (but no random error) for each $\tau_{(p_1,p_2)}^{\mathrm{corr}}$ is calculated by way of a straight-line least-squares fit to $\ln\{\mathrm{Re}(C_{(p_1,p_2)}[\tau])_{\mathrm{BV}}\}$ against Monte Carlo time displacement τ, for $\tau < K$; the value of K is the smallest integer that satisfies (i) $K < H$, (ii) $\mathrm{Re}(C_{(p_1,p_2)}[K]_{\mathrm{BV}})/F_{(p_1,p_2)} < \exp[-2] \approx 0.1353$, yet (iii) $\mathrm{Re}(C_{(p_1,p_2)}[K]_{\mathrm{BV}}) \gg \mathrm{NF}$, where NF denotes the *noise floor* of $\mathrm{Re}(C_{(p_1,p_2)}[\tau])_{\mathrm{BV}}$ (see Ref. 60). Condition (i) requires that H [see stage (SAMC 3)] be large enough. Conditions (ii) and (iii) require that G [again, see stage (SAMC 3)] be large enough. Define $\tau_{\max}^{\mathrm{corr}} \equiv \tau_{(1,0)}^{\mathrm{corr}}$ [the largest $\tau_{(p_1,p_2)}^{\mathrm{corr}}$ always corresponds to $(p_1,p_2) = (1,0)$].

A long athermal Monte Carlo (LAMC) run comprises four stages.

(LAMC 1) First, an $[I,D]$-type Stampfli approximant is constructed. This stage is identical to stage (SAMC 1).

(LAMC 2) Next, the athermal Monte Carlo step (Sec. VI A) is applied M times, where M equals the nearest integer to $4 \times \tau_{\max}^{\mathrm{corr}}$; then certain [the same as in stage (SAMC 3)] phason-mode components $\tilde{h}_i(\mathbf{k})$ are calculated for the extant approximant. The combined process (M athermal Monte Carlo steps plus calculation of phason-mode components) is then repeated $N-1$ times; N is the number of *independent samples*. Let n (a suffix) label the phason-mode components that are calculated on the nth such occasion ($1 \le n \le N$).

(LAMC 3) Next, certain best values and random errors that are defined as

$$\langle|\tilde{h}_i(\mathbf{k})|^2\rangle_{\mathrm{BV}} = \frac{1}{N}\sum_{n=1}^{N}\langle|\tilde{h}_i(\mathbf{k})_n|^2\rangle \tag{62}$$

and

$$[\langle|\tilde{h}_i(\mathbf{k})|^2\rangle_{\mathrm{RE}}]^2 = \frac{1}{N^2}\sum_{n=1}^{N}\langle|\tilde{h}_i(\mathbf{k})_n|^4\rangle - \frac{1}{N}[\langle|\tilde{h}_i(\mathbf{k})|^2\rangle_{\mathrm{BV}}]^2 \tag{63}$$

are calculated.

(LAMC 4) Finally, estimates of reduced symmetry-averaged phason-mode fluctuations $F_{(p_1,p_2)}|_{\mathrm{red}}$ are obtained, using Eqs. (53)–(56), from the best values $\langle|\tilde{h}_i(\mathbf{k})|^2\rangle_{\mathrm{BV}}$ and the random errors $\langle|\tilde{h}_i(\mathbf{k})|^2\rangle_{\mathrm{RE}}$ that are calculated in stage (LAMC 3).

Sundry details apropos stages (LAMC 2) and (LAMC 3): The phason modes of the Stampfli approximant that is constructed in stage (LAMC 1) are extremely small and unrepresentative of random $[I,D]$-type square-triangle approximants. As a result, they do not enter the sums on the right-hand sides of Eqs. (62) and (63); that is, the (discrete) range of the index n omits $n = 0$. The first M athermal Monte Carlo steps that are applied in stage (LAMC 2) *equilibrate* the Stampfli approximant to a random square-triangle approximant, whose phason modes, which are representative of random $[I,D]$-type square-triangle approximants, do enter the sums; that is, the range of the index n includes $n = 1$. Equation (63) implicitly assumes that M athermal Monte Carlo steps are sufficient to decorrelate completely every phason mode. Note that phason-mode fluctuations are estimated in parallel [fact (i) of Sec. VI C and the need for computational efficiency motivate this]. In practice, stages (LAMC 2) and (LAMC 3) and done in tandem (i.e., running totals are calculated), thereby avoiding the need to store (in the memory of the computer) large numbers of phason-mode components.

F. Results: phason-mode autocorrelation functions

With the array dimension $D = 1$, E [see Sec. VI E, stage (SAMC 2)] $= 10^5$ (to beg no questions apropos equilibration—see Ref. 59), G [see Sec. VI E, stage (SAMC 3)] $= 10^6$, and H [see Sec. VI E, stage (SAMC 3)] $= 100$, short athermal Monte Carlo runs were performed for inflation orders $I = 1$, 2, and 3. Every symmetry-averaged phason-mode autocorrelation function $C_{(p_1,p_2)}[\tau]$ appeared to decay exponentially (down to a noise floor–note Ref. 60); see Fig. 7.

A one-parameter least-squares fit (see Fig. 8) to the best values for $\tau_{(p_1,p_2)}^{\mathrm{corr}}$ that were obtained from the short athermal Monte Carlo run for which $[I,D] = [3,1]$ [see Eq. (61); for the purposes of the fit, the value of B, which

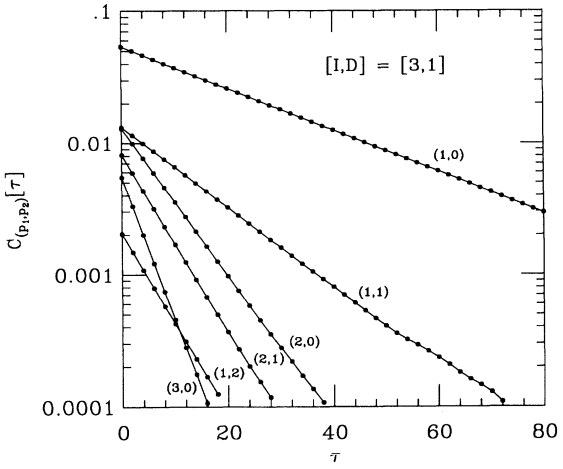

FIG. 7. Best values of symmetry-averaged phason-mode autocorrelation functions $C_{(p_1,p_2)}[\tau]$, for $[I,D] = [3,1]$, against Monte Carlo time displacement τ. Each line [labelled by (p_1,p_2)] joins estimates of the same $C_{(p_1,p_2)}[\tau]$ at different values of τ. The unit of Monte Carlo time is an athermal Monte Carlo step (see Sec. VI A). Because the ratio C [see Eq. (52)] is usually close to 1, the trial tiling of an athermal Monte Carlo step is almost always accepted; a single zipper update move thus typically rearranges many squares and triangles.

equals $1/\lambda^6 \approx 3.7 \times 10^{-4}$, is taken to be zero; y (no error bars) $= cx/(\Gamma K_\mu)$, where $y = \tau^{\rm corr}_{(p_1,p_2)}$, $c = L^2/(4\pi^2)$, and $x = 1/(p_1^2 + p_2^2)$] gives

$$\Gamma K_\mu = 0.01250 \pm 0.00048. \tag{64}$$

With $I = 1$, $E = 10^4$, $G = 10^5$, and $H = 100$, short athermal Monte Carlo runs were performed for $D = 2$, . . . , 16. See Fig. 9; the largest autocorrelation time $\tau^{\rm corr}_{\rm max}$,

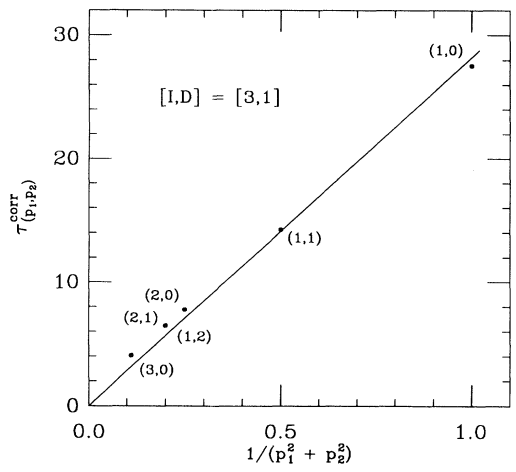

FIG. 8. Best values of autocorrelation times $\tau^{\rm corr}_{(p_1,p_2)}$, for $[I,D] = [3,1]$, against $1/(p_1^2 + p_2^2)$. The straight line shown is the best-fit line for the estimation of ΓK_μ (see Secs. VI D and VI F). [The best values that correspond to $(p_1,p_2) = (2,1)$ and (2,1) lie almost exactly on top of one another (they differ by only 0.016).]

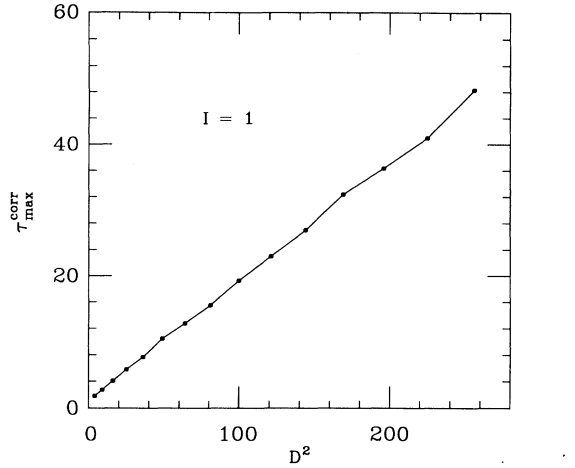

FIG. 9. Best values of largest autocorrelation times $\tau^{\rm corr}_{\rm max}$, against array dimension squared D^2, with the inflation order I set to 1, and the array dimension $D = 2, 3, \ldots, 16$.

which corresponds to $|\mathbf{k}| = 2\pi/L$, appears to scale proportionally to $L^2 = D^2\lambda^2$—just as Eq. (61) predicts. From Secs. VI A and VI B, the average amount of computer time that is needed to execute the zipper update move (Sec. IV) and the amount of computer time that is needed to decide whether to accept or reject a zipper, both scale proportionally to L^2. Hence, the amount of computer time that equates to the largest autocorrelation time $\tau^{\rm corr}_{\rm max}$ scales proportionally to L^4, and the amount of computer time that is needed to perform a long athermal Monte Carlo run scales proportionally to NL^4 [the quantity N is the number of independent samples; see Sec. VI E, stage (LAMC 2)].

G. Results: phason-mode fluctuations (estimation of K_μ, Γ, and J)

Note that, as the inflation order I grows, with the array dimension $D = 1$, (i) $L = \lambda^I$ tends to infinity [this follows from Eq. (45)], (ii) $B = 1/\lambda^{2I}$ tends to zero [this follows from Eq. (47)], and (iii) [a consequence of (ii)] every reduced symmetry-averaged phason-mode fluctuation $F_{(p_1,p_2)}|_{\rm red}$ tends to a common value that equals $1/K_\mu$ [see Eq. (56)]. With the array dimension $D = 1$, long athermal Monte Carlo runs were performed for inflation orders $I = 1$, 2, and 3. (The run for $I = 3$ required about 19 h of computer time on an IBM RS-6000.) See Table I; note that, for small L (that is, for $I = 1$; $L = \lambda \approx 3.732$), the estimates of reduced symmetry-averaged phason-mode fluctuations are huge and do not fit Eq. (56). Such behavior should not be surprising: The continuum theory (Sec. III), upon which Eq. (56) is based, is only valid for $L \gg 1$ and $|\mathbf{k}| \ll 1$. For $D = 1$, this *finite-L noise* overwhelms, for any I, the effect that a finite B has on the magnitudes of reduced symmetry-averaged phason-mode fluctuations $F_{(p_1,p_2)}|_{\rm red}$.

A one-parameter (K_μ) least-squares fit to the estimates of symmetry-averaged phason-mode fluctuations,

TABLE I. Results of athermal Monte Carlo runs: I is the inflation order; D is the array dimension; M is the number of Monte Carlo steps that separate the times when phason-mode components were calculated [see Sec. VI E, stage (LAMC 2)]; N is the total number of such times, i.e., the number of independent samples; each reduced symmetry-averaged phason-mode fluctuation [i.e., each $F_{(p_1,p_2)}|_{\rm red}$—see Eqs. (53)–(55)] is specified by p_1, p_2, I, and D.

	$[I,D]=[1,1]$ $M=2$ $N=1\times10^6$	$[I,D]=[2,1]$ $M=12$ $N=8\times10^4$	$[I,D]=[3,1]$ $M=110$ $N=6\times10^3$	$[I,D]=[1,16]$ $M=193$ $N=6\times10^3$
$[p_1,p_2]$	Estimate of $F_{(p_1,p_2)}\|_{\rm red}$			
[1,0]	$(1.278\pm0.002)\times10^2$	2.173 ± 0.008	2.174 ± 0.028	2.932 ± 0.038
[1,1]	$(3.827\pm0.005)\times10^3$	2.317 ± 0.008	2.163 ± 0.028	1.635 ± 0.021
[2,0]	$(2.187\pm0.004)\times10^4$	2.528 ± 0.009	2.146 ± 0.027	2.951 ± 0.038
[2,1]	$(1.436\pm0.003)\times10^5$	2.600 ± 0.009	2.189 ± 0.028	1.906 ± 0.025
[3,0]	$(1.901\pm0.003)\times10^6$	5.105 ± 0.027	2.178 ± 0.028	3.012 ± 0.039
[1,2]	$(5.746\pm0.013)\times10^5$	3.521 ± 0.016	2.189 ± 0.028	1.906 ± 0.025

for $[I,D]=[3,1]$, that appear in Table I [see Eq. (56); for the purposes of the fit, the value of B, which equals $1/\lambda^6\approx3.7\times10^{-4}$, is taken to be zero; y (with error bars) $=cK_\mu x$, where $y=1/F_{(p_1,p_2)}$, $c=4\pi^2/L^2$, and $x=(p_1^2+p_2^2)^2/p_1^2$] gives

$$K_\mu=0.4602\pm0.0024. \tag{65}$$

Equations (64) and (65) give

$$\Gamma=0.0272\pm0.0010. \tag{66}$$

Note that, as the array dimension D grows, with the inflation order $I=1$, (i) $L=D\lambda$ tends to infinity [see Eq. (45)], but now (ii) $B=1/\lambda^2$ remains constant [see Eq. (47)], equal to $(1-\sqrt{3}/2)/(1+\sqrt{3}/2)\approx0.07180$, and (iii) reduced symmetry-averaged phason-mode fluctuations tend to nondegenerate (since $B\neq0$) values [see Eq. (56)].

With the inflation order $I=1$, athermal Monte Carlo runs were performed for array dimensions D equal to 2,3,...,16. See Fig. 10; note that, as D increases, the finite-L noise diminishes and, as a result, the effect of a finite B, that is, the nondegeneracy of the reduced symmetry-averaged phason-mode fluctuations [see Eq. (56)], becomes apparent.

A long athermal Monte Carlo run was performed for $[I,D]=[1,16]$, with $N=6000$. (This run required about 25 h of computer time on an IBM RS-6000.) A two-parameter (K_μ and J) least-squares fit to the estimates of symmetry-averaged phason-mode fluctuations that were thereby obtained [Table I (rightmost column)] [y (with error bars) $=cx_1(K_\mu+Jx_2)$, where $y=1/F_{(p_1,p_2)}$, $c=4\pi^2/L^2$, $x_1=(p_1^2+p_2^2)^2/p_1^2$, and $x_2=2B\cos(4\theta_{\mathbf{k}})$] gives (see Fig. 11) $K_\mu=0.4795\pm0.0029$, and

$$J=-0.987\pm0.022. \tag{67}$$

The discrepancy that exists between the above estimate of K_μ and Eq. (65) is perhaps due either to finite-size effects or to the approximations that the continuum theory (Sec. III) makes (higher-order terms are excluded from the entropy density), or to both.

VII. ENTROPIES VIA MONTE CARLO SIMULATIONS

This section motivates, then describes, how the authors obtained an estimate of the entropy per unit area of infinite square-triangle tilings at zero (background) phason strain [i.e., s_a^r—see Eq. (12)] and, as a by-product, a crude estimate of the second-order elastic constant K_ξ [see Eq. (14)]. (Because K_ξ couples to a term in the entropy density that is a total divergence [see Eq. (22)], it cannot be estimated by measuring phason-mode fluctuations.)

At this point, the authors express some opinions. In any calculation, the "human factor" cannot be ignored.

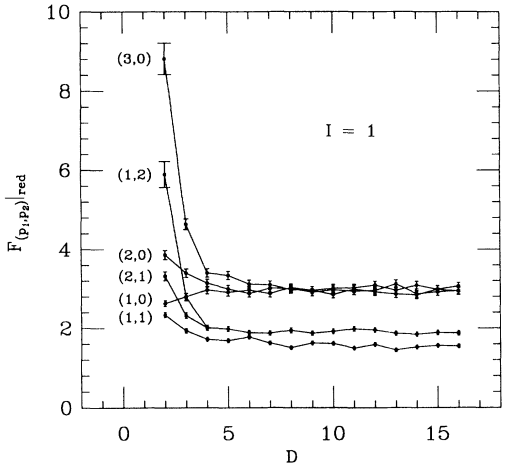

FIG. 10. Separating the effects of a finite background phason strain from finite-L effects: Estimates of reduced symmetry-averaged expectations $F_{(p_1,p_2)}|_{\rm red}$, with the inflation order I set to 1, and the array dimension $D=2,3,\ldots,16$. The background phason strain $\underline{B}$ that corresponds to $I=1$ takes the form of Eq. (19), with $B=(1-\sqrt{3}/2)/(1+\sqrt{3}/2)\approx0.07180$. The side length L of a unit cell is directly proportional to D—see Eq. (45). Each line [labeled by (p_1,p_2)] joins estimates of the same $F_{(p_1,p_2)}|_{\rm red}$ for different values of D.

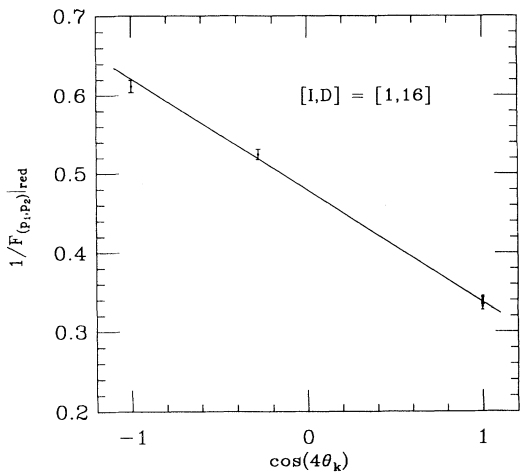

FIG. 11. How well does the continuum theory (Sec. III) explain the effects of a finite background phason strain? Estimates of inverse reduced symmetry-averaged phason-mode fluctuations $[1/F_{(p_1,p_2)}|_{red}$—see Eq. (55)], for $[I,D] = [1,16]$, with $N = 6000$, are plotted against $\cos(4\theta_k)$ [this quantity multiplies $2JB$ in Eq. (56)]. The straight line shown is a least-squares fit to these estimates (see Sec. VI G, last paragraph); the intercept at $\cos(4\theta_k) = 0$ estimates K_μ; the slope estimates $2BJ$. Equation (67) displays the estimate of J that is thereby obtained [$B = (1-\sqrt{3}/2)/(1+\sqrt{3}/2)$]. For this fit (see Ref. 61): The number of estimates equals 6; the number of free parameters equals 2; the number of degrees of freedom equals $6 - 2 = 4$; the chi square $\chi^2 = 5.139$; the chi-square probability Q (a measure of the goodness of fit) $= 0.2733$. The value of the latter quantity means (modulo the tacit assumption of normal statistics) that the continuum theory fits the results reasonably well—see Ref. 61.

A method's power depends not just on its efficiency, but also on its facility; these two qualities are often antagonists. Transfer-matrix methods are, by and large, more efficient (as regards computer time) than Monte Carlo methods for estimating the entropy per unit area of random tilings. Also, Monte Carlo methods are inherently more cumbersome than transfer-matrix methods because they involve random errors. By using maps that identify random tilings with spin configurations (see Sec. VIII), transfer-matrix calculations (that is, the construction of transfer matrices—or whatever, in practice, equates to this task—and the calculation of largest eigenvalues) for two-dimensional random tilings can be implemented on a computer without too much difficulty. The construction of transfer matrices for three-dimensional random tilings, however, is far more difficult.[62] Though such transfer matrices can be built, by hand, for systems that correspond to quite small background phason strains, the task is extremely laborious.

Monte Carlo methods, in contrast, use a computer's labor to generate estimates of phason-mode fluctuations, from which estimates of certain elastic constants can be obtained (see Refs. 8, 9 and 37 and Sec. VI of this paper). Other—different though related—Monte Carlo methods produce estimates of total entropies for ensembles comprising random tilings, from which an estimate of the entropy per unit area (or, equivalently, the entropy per vertex or the entropy per tile) at zero (background) phason strain and estimates of the elastic constants[64] can be obtained (see Refs. 10 and 63 and Sec. VII of this paper). The latter Monte Carlo methods, however, are tedious—both from a human and from a computational prospective; they should be implemented only when all else (transfer-matrix methods, mean-field theories—see Ref. 2) fails. A Monte Carlo method for estimating total entropies is presented below (Secs. VII B–VII E); it is the most efficient method of its type. The task of implementing it, moreover, is no more difficult—and is, in many ways, less irksome—than the task of implementing any one of the alternative Monte Carlo methods (see Ref. 65). The method contains two vital ingredients: a *pseudo-Hamiltonian*, which defines canonical ensembles of random tilings, and an adaptation of the Ferrenberg-Swendsen histogram method.[67]

This section is organized as follows: Section VII A surveys the various Monte Carlo methods for estimating the total entropies of maximally random ensembles that comprise random tilings [much (but not all) of this subsection is unrelated to the subsections that follow it]. Section VII B describes the authors' adaptation and implementation of the Ferrenberg-Swendsen histogram method. Section VII C defines a pseudo-Hamiltonian for $[I,D]$-type square-triangle approximants, then describes the structure (ground states, excited states) of the canonical ensembles that this pseudo-Hamiltonian engenders. Section VII D defines the thermal equivalent of the athermal Monte Carlo step (Sec. VI A). Section VII E details the inner workings of a thermal Monte Carlo run. Section VII F presents results (energy histograms and estimates of entropies), then explains how estimates of s_a^r and K_ξ were obtained by way of *ad hoc* finite-size scaling.

A. Survey of methods

Reference 68 contains a broad review of the known Monte Carlo methods for estimating the free energies and/or entropies of statistical systems. Monte Carlo methods can be divided into two classes: (i) *athermal* methods, which (a) do not invoke a (pseudo-)Hamiltonian and (b) use an athermal Monte Carlo step that satisfies detailed balance for maximally random ensembles (Sec. VI A describes a Monte Carlo step of this sort); (ii) *thermal* methods, which (a) do invoke a (pseudo-)Hamiltonian and (b) use a thermal Monte Carlo step that satisfies detailed balance for canonical ensembles (Sec. VII D describes a Monte Carlo step of this, the latter, sort).

To the authors' knowledge, only one athermal Monte Carlo method is at all useful for estimating the total entropies of (maximally random) ensembles that comprise random tilings: Ma's coincidence-counting method.[69–71] Though elegant from a conceptual standpoint, Ma's method can only estimate total entropies for small unit cells.[72] To check detailed balance, to verify the estimates of total entropies that were obtained through thermal Monte Carlo methods, and to satisfy their curiosities, the

authors implemented Ma's method for random square-triangle tilings (viz., for maximally random ensembles comprising $[I, D]$-type approximants); see Appendix C.

Three more-or-less distinct thermal Monte Carlo methods are useful for estimating the total entropies of ensembles that comprise random tilings: the *energy method*, the *variance method*, and the *histogram method*. The remainder of this subsection first explains the idea on which all three methods are based; the energy and variance methods are then described in brief; finally, the merits and/or shortcomings of the energy and variance methods are discussed (the histogram method is described and discussed in Sec. VII B).

Consider a maximally random ensemble comprising $\mathcal{N}_m$ *microstates*. Suppose that the value of the total entropy $\ln[\mathcal{N}_m]$ is desired, but that no analytic-combinatoric method exists for calculating it. Now imagine a canonical ensemble comprising the same microstates, at a temperature T, where a pseudo-Hamiltonian assigns the ith microstate an energy U_i. In this ensemble, the ith microstate occurs with a probability

$$p_i(T) = \frac{\exp[-U_i/T]}{Q(T)}; \tag{68}$$

the authors take Boltzmann's constant k_B to equal unity. The partition function of the ensemble is

$$Q(T) = \sum_{i=1}^{\mathcal{N}_m} \exp[-U_i/T]; \tag{69}$$

the expected energy over the ensemble is

$$\langle U \rangle_T = \sum_{i=1}^{\mathcal{N}_m} p_i(T) U_i; \tag{70}$$

the (total) entropy of the ensemble, by the Gibbs entropy formula, is

$$S(T) = -\sum_{i=1}^{\mathcal{N}_m} p_i(T) \ln[p_i(T)]. \tag{71}$$

At infinite temperature ($T = \infty$), every microstate occurs with the same probability, which equals $1/\mathcal{N}_m$ [see Eqs. (68) and (69)]. The total entropy at infinite temperature, i.e., $S(\infty)$, thus equals $\ln[\mathcal{N}_m]$. On the other hand, the total entropy at zero temperature, i.e., $S(0)$, is the total entropy of the *ground state*, a.k.a. the *residual* (total) entropy. Suppose that, by a judicious choice of pseudo-Hamiltonian, the latter entropy [viz., $S(0)$], unlike $S(\infty)$, is either zero or calculable by some analytic-combinatoric means. An estimate of the total entropy $\ln[\mathcal{N}_m]$ can then be obtained by estimating $[S(\infty) - S(0)]$ via thermal Monte Carlo simulations.[73] Note that the pseudo-Hamiltonian is merely a technical device that smoothly transforms the ground state, the value of whose entropy is known, into the maximally random ensemble, the value of whose entropy is desired; the pseudo-Hamiltonian thus need not be physical.

Using Eqs. (68)–(71), the relation

$$\frac{dS(T)}{dT} = \frac{1}{T}\frac{d\langle U \rangle_T}{dT} \tag{72}$$

can be derived. Integrating with respect to T, between 0 and ∞, gives

$$S(\infty) - S(0) = \int_0^\infty \frac{1}{T}\frac{d\langle U \rangle_T}{dT}\, dT. \tag{73}$$

Now, Eq. (73) is the basis of the first thermal Monte Carlo method (i.e., the *energy method*): Find estimates of the expected energy $\langle U \rangle_T$ for a discrete range of temperatures T between 0 and ∞; then estimate $[S(\infty) - S(0)]$ via numerical differentiation (to find $d\langle U \rangle_T / dT$) and subsequent numerical integration.

Using Eqs. (68)–(70), the relation

$$\frac{d\langle U \rangle_T}{dT} = \frac{1}{T^2}(\langle U^2 \rangle_T - \langle U \rangle_T^2) \tag{74}$$

can be derived. Substituting Eq. (74) into Eq. (73) gives

$$S(\infty) - S(0) = \int_0^\infty \frac{C(T)}{T}\, dT, \tag{75}$$

where $C(T)$, the heat capacity, equals $(\langle U^2 \rangle_T - \langle U \rangle_T^2)/T^2$. Now, Eq. (75) is the basis of the second thermal method (i.e., the *variance method*): Find estimates of the heat capacity $C(T)$ for a discrete range of temperatures T between 0 and ∞; then estimate $[S(\infty) - S(0)]$ via numerical integration.

Using the variance method, Orrick[63] estimated the entropy per tile of random eightfold-symmetric rhombus tilings. Reference 74 gives raw Monte Carlo data [both the expected energy against temperature and the specific heat (heat capacity per tile) against temperature] for systems involving random tenfold-symmetric rhombus (viz., two-dimensional Penrose) tilings. Strandburg[10] estimated the entropy per tile of random three-dimensional Penrose tilings by way of the variance method, integrating a smoothing-spline fit to her Monte Carlo data for the specific heat against temperature. Using the energy method, the authors obtained a rough estimate of the entropy per unit area at zero phason strain (s_a^r) for random square-triangle tilings.[66]

Because it avoids numerical differentiation, the variance method is somewhat easier to implement than the energy method. The specific heat, however, exhibits *lack of spatial self-averaging* (see Refs. 52 and 75). Thus, the suitability of the variance method, as regards estimating total entropies for systems whose unit cells are large, is somewhat suspect [the only way to reduce the random error of an estimate would be to increase the number of Monte Carlo steps (that is, the number of independent samples)]. A reliable and accurate estimate of the entropy per unit area at zero phason strain requires estimating total entropies for systems that correspond to low background phason strains, whose unit cells are necessarily large. Unlike the specific heat, the expected energy per unit area (or per vertex or per tile) does exhibit spatial self-averaging. Hence, the energy method, though somewhat more awkward to implement, should be the better (vis-à-vis the variance method—see Ref. 76), as

regards estimating total entropies for systems whose unit cells are large.

Note that the factor of $1/T$ in the integrand of Eq. (73) makes the integral particularly sensitive to the low-T behavior of $\langle U\rangle_T$. Similarly, the factor of $1/T^3$ [including the factor of $1/T^2$ from the definition of $C(T)$] in the integrand of Eq. (75) makes the integral extremely sensitive to the low-T behavior of $(\langle U^2\rangle_T - \langle U\rangle_T^2)$. If the (thermal) Monte Carlo dynamics slows down (that is, if the characteristic times of autocorrelation functions diverge) as $T \to 0$, as would happen if an energy gap were present between the ground state(s) and the first-excited states, then both $\langle U\rangle_T$ and $(\langle U^2\rangle_T - \langle U\rangle_T^2)$ are hard to estimate at the very temperatures where accurate estimates are most needed.

B. Histogram method

The third thermal Monte Carlo method, i.e., Ferrenberg and Swendsen's *histogram method*,[67] is now described. Consider a canonical ensemble, at a temperature T, comprising tilings whose energies occupy (more for convenience than necessity) discrete, equally spaced energy levels. Next, consider a sequence of length $\mathcal{N}$, which comprises certain members of this ensemble, that is generated by way of a (well-formulated) thermal Monte Carlo step. Now imagine the *energy histogram* of such a sequence, where the height of the lth bar in the histogram equals the number of tilings in the sequence whose energies occupy the lth energy level. The expected height of the lth bar is given by

$$\langle H_l(T)\rangle = \mathcal{N} p_l(T) W_l, \tag{76}$$

where W_l is the number of distinct tilings whose energies occupy the lth energy level, and $p_l(T)$—whose mathematical definition takes the same form as Eq. (68)—is the probability with which each such tiling occurs; W_l, as a function of l, is the *density of states*. The Ferrenberg-Swendsen histogram method has an ancestry that dates back at least to the use of *bridging distributions* by Valleau and Card.[77] It affords an efficient way to estimate $[S(\infty) - S(0)]$ from a finite number of histograms, whose corresponding temperatures cover a discrete range; these histograms should overlap to form a *bridge* between the histogram corresponding to $T = 0$ [viz., $\langle H_l(0)\rangle$ equals $\mathcal{N}$, if $l = 0$, but zero otherwise] and the histogram corresponding to $T = \infty$ (viz., $\langle H_l(\infty)\rangle = \mathcal{N} W_l / \exp[S(\infty)] \propto$ the density of states). At this point, the authors direct the reader to Ferrenberg and Swendsen's paper.[67]

A way to unify, in some sense, all three thermal Monte Carlo methods is to consider the cumulant expansions of energy histograms: The energy method uses the first-order cumulants of energy histograms. The variance method uses the second-order cumulants of energy histograms. The histogram method, however, uses complete histograms, i.e., all of the cumulants. This explains why the histogram method is the most efficient: It uses all of the available information.

A necessary component of any Monte Carlo method is a procedure for finding random errors (uncertainties). For the histogram method, this procedure concerns the random errors of expected bar heights. Consider the above sequence of $\mathcal{N}$ tilings. The best value for the expected height of the lth bar in the histogram is given by

$$\langle H_l(T)\rangle_{\mathrm{BV}} = n_l, \tag{77}$$

where n_l is the number of tilings in the sequence whose energies occupy the lth energy level. Assuming that the relevant autocorrelation function (see below) decays exponentially, the random error of the above best value is given by

$$[\langle H_l(T)\rangle_{\mathrm{RE}}]^2 = (1 + 2\tau_l^{\mathrm{corr}})\langle H_l(T)\rangle_{\mathrm{BV}}, \tag{78}$$

where τ_l^{corr} is the autocorrelation time for the lth bar. Note that Eq. (78) differs somewhat from Ferrenberg and Swendsen's equivalent: In their paper, τ^{corr} does not depend on the energy level l. Let $e(\tau)$ be the energy level of the random tiling extant at Monte Carlo time τ ($e = 0$ corresponds to a ground-state tiling; $e = n$ corresponds a tiling whose energy occupies the nth energy level). Define $c_l[e]$ as the function that equals unity if $e = l$, but zero otherwise. Denote the long-time average of $c_l[e(\tau)]$ as $\langle c_l\rangle$. Assume that the autocorrelation function of $c_l[e(\tau)]$, viz., $\langle c_l[e(\tau)]c_l[e(0)]\rangle - \langle c_l\rangle^2$, decays exponentially. The autocorrelation time for the lth bar can then be defined through the normalized autocorrelation function of $c_l[e(\tau)]$:

$$\begin{aligned}\langle c_l[e(\tau)]c_l[e(0)]\rangle_{\mathrm{norm}} &\equiv \frac{\langle c_l[e(\tau)]c_l[e(0)]\rangle - \langle c_l\rangle^2}{\langle c_l^2\rangle - \langle c_l\rangle^2} \\ &= \exp[-\tau/\tau_l^{\mathrm{corr}}],\end{aligned} \tag{79}$$

where $\langle c_l^2\rangle$ is the long-time average of $c_l[e(\tau)]^2$. A best value for each τ_l^{corr} is obtained by calculating best values for $\langle c_l[e(\tau)]c_l[e(0)]\rangle_{\mathrm{norm}}$ at various Monte Carlo time displacements τ, then fitting Eq. (79) (one parameter: τ_l^{corr}) to these best values [see Sec. VII E, stage (TMC 3)]; the random error $\langle H_l(T)\rangle_{\mathrm{RE}}$ is then calculated using Eq. (78). The modifications to Ferrenberg and Swendsen's error analysis that are necessary to incorporate the l dependence of τ_l^{corr} are straightforward.

C. Pseudo-Hamiltonian and its Stampfli ground states

The definition of the pseudo-Hamiltonian that the authors actually used [Eqs. (83) and (84) below] involves *rationally related* perp.-space basis vectors, custom designed for $[I, D]$-type square-triangle approximants. These basis vectors are defined as

$$\begin{aligned}\bar{\mathbf{e}}_0^{\perp} &= (\ 1\ ,\ 0\ )^{\perp}, \\ \bar{\mathbf{e}}_1^{\perp} &= (\ -r_I\ ,\ -\tfrac{1}{2}\ )^{\perp}, \\ \bar{\mathbf{e}}_2^{\perp} &= (\ \tfrac{1}{2}\ ,\ r_I\ )^{\perp}, \\ \bar{\mathbf{e}}_3^{\perp} &= (\ 0\ ,\ -1\ )^{\perp},\end{aligned}, \tag{80}$$

where $r_I \equiv a_I/b_I$, and

$$\begin{bmatrix} a_I \\ b_I \end{bmatrix} = \begin{bmatrix} 2 & \frac{3}{2} \\ 2 & 2 \end{bmatrix}^I \begin{bmatrix} 1 \\ 0 \end{bmatrix}. \tag{81}$$

Note that a_I and b_I (thus r_I) are independent of D and that $r_I = \{1, \frac{7}{8}, \frac{13}{15}, \ldots\}$ are rational approximants of $\sqrt{3}/2$.

The rationally related perp.-space position vector of a vertex v in an $[I, D]$-type square-triangle approximant is defined as

$$\bar{\mathbf{f}}_v = \sum_{i=0}^{3} n_i \bar{\mathbf{e}}_i^{\perp}, \tag{82}$$

where the n_i are the same n_i as appear in Eq. (1). The modified perp.-space position vector $\tilde{\mathbf{f}}_v$ [see Eq. (24)] of the vertex v is related to $\bar{\mathbf{f}}_v$ by a scale transformation $\tilde{\mathbf{f}}_v = (1 - B)\bar{\mathbf{f}}_v$, where B is given by Eq. (47). The reasons for using rationally related perp.-space position vectors as opposed to using modified perp.-space position vectors are purely technical—see Ref. 78; the same effect (that of subtracting out the background phason strain) is achieved through the use of either.

The (*perp.-space variance*) pseudo-Hamiltonian that the authors used is now defined: The energy U of an $[I, D]$-type approximant is

$$U = \sum_{n=1}^{N_v} |\bar{\mathbf{f}}_{v_n} - \langle \bar{\mathbf{f}}_v \rangle|^2, \tag{83}$$

where N_v is the number of vertices that the approximant contains, $\bar{\mathbf{f}}_{v_n}$ is the rationally-related perp.-space position vector of the nth vertex in the approximant, and $\langle \bar{\mathbf{f}}_v \rangle$, the average rationally related perp.-space position vector, is defined as

$$\langle \bar{\mathbf{f}}_v \rangle = \frac{1}{N_v} \sum_{n=1}^{N_v} \bar{\mathbf{f}}_{v_n}. \tag{84}$$

Note that U is invariant under overall translations in perp. space. The authors stress that the pseudo-Hamiltonian is a technical device; Eqs. (83) and (84) require no physical justification and/or interpretation. Orrick[63] and Strandburg[10] both used the pseudo-Hamiltonian defined as

$$U' = \sum_{n=1}^{N_v} |\bar{\mathbf{f}}_{v_n}|^2; \tag{85}$$

that is, they omitted the counter term $\langle \bar{\mathbf{f}}_v \rangle$. The latter pseudo-Hamiltonian (U') is sensitive to overall translations in perp. space; Ref. 79 discusses a consequence of this sensitivity.

Consider a canonical ensemble that comprises $\mathcal{N}_r(I, D)$ random $[I, D]$-type approximants and which contains, as a subensemble, $\mathcal{N}_S(I, D)$ Stampfli tilings [$\mathcal{N}_S(I, D) \leq \mathcal{N}_r(I, D)$]. Every approximant in this ensemble contains $N_v(I, D)$ vertices. With the above pseudo-Hamiltonian [Eqs. (83) and (84)], the subensemble of Stampfli tilings forms the (degenerate) ground state of the canonical ensemble. Thus, the entropy of the canonical ensemble at $T = 0$ is $S^S[I, D]$; see Eq. (51). The histogram method was used (Sec. VII F) to obtain estimates of $(S^r[I, D] - S^S[I, D]) = \ln[\mathcal{N}_r(I, D)/\mathcal{N}_S(I, D)]$ for various inflation orders I and array dimensions D. The remainder of this subsection concerns the ground states (Stampfli tilings) and the excited states (non-Stampfli tilings) that the pseudo-Hamiltonian defines; it can be skipped without loss of continuity.

The degeneracy of a Stampfli subensemble can be proved by noting that the right-hand side of Eq. (83) is the vertices' *moment of inertia* in perp. space. This paragraph attempts, in words, to explain a proof. Imagine the relevant *inflation tree* of Stampfli tilings (i) whose *root* is a $D \times D$ array of squares, (ii) whose *leaves* are Stampfli tilings, and (iii) whose topmost leaves—the inflation tree's *canopy*—compose the Stampfli subensemble. Unlike random square-triangle tilings, Stampfli tilings contain *patterns*. A pattern is a region of a Stampfli tiling, whose (the region's) outline is both 12-fold symmetric and dependent only on the pattern's *order*. Two distinct first-order patterns exist; they both comprise 6 squares and 12 triangles; their common outline is a regular dodecagon with unit side length [note Sec. V A, parts (RS 2) and (RS 3)]. The $(m+1)$th-order patterns are related to the mth-order patterns by a (random-)Stampfli inflation (see Sec. V A). An mth-order *leap* is the rotation of an mth-order pattern, by 30°, about the vertex at the pattern's center. A first-order leap connects (in the authors' technical sense of the word—see Sec. IV) two Stampfli tilings, in the inflation tree's canopy, that are siblings. A higher-order leap connects two Stampfli tilings, in the inflation tree's canopy, that are more distantly related. Every leap, however, corresponds to a first-order leap within a Stampfli tiling (a leaf) that resides somewhere in—at some (not necessarily the topmost) level of—the inflation tree. Consider the vertices that lie within the outline of a pattern. By symmetry, their perp.-space *center of mass* coincides with the vertex at the pattern's center; it (the perp.-space center of mass) is thus invariant under the leap that rotates the pattern. Now consider all of the vertices that a Stampfli tiling contains; their perp.-space center of mass is also invariant under the same leap; this follows from the perp.-space analog of the *parallel-axis theorem* in elementary mechanics. Thus, every Stampfli tiling in the subensemble has the same perp.-space moment of inertia and, as a result (for the above pseudo-Hamiltonian [Eqs. (83) and (84)]), the same energy.

The non-Stampfli tilings (approximants) that compose the above canonical ensemble have energies that occupy discrete energy levels, at integer multiples of a constant energy-level spacing Δ above the ground-state energy (i.e., the energy levels form a ladder). The authors found (from energy histograms) that

$$\Delta(I, D) = \frac{x(I)y(D)}{b_I^2}; \tag{86}$$

$x(I)$ equals N_v/D^2 [see Eqs. (48) and (49)]; $y(D)$ equals 1(2), if D is even(odd); b_I is defined by Eq. (81). Now, as $I \to \infty$, $x(I)/b_I^2 \to \frac{1}{2}(3 + 2\sqrt{3})$; recall that $B = 1/\lambda^{2I}$; the energy-level spacing (for even D) at zero background phason strain is thus

$$\Delta_{B=0} = \tfrac{1}{2}(3 + 2\sqrt{3}). \quad (87)$$

Low-excited states are essentially Stampfli approximants with defective regions. The authors found each first-excited state to be a *once-deflated* approximant (edge lengths equal to λ), whose constituent *big* squares, big triangles, and two big thin rhombi are decorated with squares and triangles; see Fig. 12. Beyond first-excited states, the authors know little about the general features and/or systematics of excitations. The taxonomy of excited states is a frontier that might hold some mathematical interest.

D. Thermal Monte Carlo step

The *thermal Monte Carlo step* that was used is identical to the athermal Monte Carlo step of Sec. VI A, except that the ratio C [see Eq. (52)] is redefined as

$$C = \frac{N_h}{N'_h} e^{(U-U')/T}, \quad (88)$$

where U and U' are the energies of the original and the trial square-triangle tilings, respectively, and T is the temperature. The athermal Monte Carlo step of Sec. VI A can be regarded as the $T \to \infty$ limit of the above thermal Monte Carlo step, wherein the energies of tilings are irrelevant. The thermal Monte Carlo step satisfies detailed balance, and as a result, a canonical ensemble of (random) square-triangle tilings [defined by Eq. (68)] is stationary under it (again, see Refs. 51 and 52). A proof of detailed balance is given in Appendix B.

E. Thermal Monte Carlo runs

A *thermal Monte Carlo (TMC) run* comprises five stages.

(TMC 1) First, an $[I, D]$-type Stampfli approximant is constructed (see Sec. V C). The inflation constant I and the array dimension D specify the system (viz., the canonical ensemble of $[I, D]$-type square-triangle approximants) that the thermal Monte Carlo run samples.

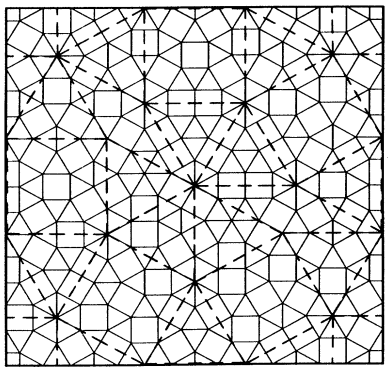

FIG. 12. Typical first-excited (with respect to the perp.-space variance pseudo-Hamiltonian [viz., Eqs. (83) and (84)]) [2, 1]-type square-triangle approximant (solid lines) and its once-deflated approximant (dashed lines), which comprises 6 big squares, 16 big triangles, and 2 big thin rhombi.

(TMC 2) Next, the thermal Monte Carlo step is applied 2^Q times at a temperature T, where Q is an integer and 2^Q is many times greater than the largest autocorrelation time τ^{corr} (see Sec. VII B). This stage merely equilibrates the system.

(TMC 3) The thermal Monte Carlo step is then applied P times, at the same temperature T as stage (ii). After each step, the energy of the extant approximant is calculated, the running total for the corresponding bar height is thereupon incremented, and then the energy is stored in a memory loop, which holds the 2^Q most recent energies. The contents of the memory loop are used to calculate best values for autocorrelation functions (see Sec. VII B) at Monte Carlo time displacements $\tau = 2^q$, where $q = 1, 2, \ldots, Q$. At the end of this stage, a best value (but no random error) for each autocorrelation time τ_l^{corr} is calculated via a straight-line fit to $\ln\{(\langle c_l[e(\tau)]c_l[e(0)]\rangle_{\text{norm}})_{\text{BV}}\}$ against τ. Estimates (best value $\pm$ random error) of expected bar heights $\langle H_l(T)\rangle$ are then calculated using Eqs. (77) and (78).

(TMC 4) Stages (TMC 2) and (TMC 3) are then repeated for different temperatures, until a solid bridge of (overlapping) energy histograms (see Fig. 13) is built between the energy histogram for $T = 0$ (i.e., the bar corresponding to $l = 0$) and the energy histogram for $T = \infty$ (i.e., the density of states W_l). (The discrete range of temperatures that were actually used is stated in Sec. VII F.]

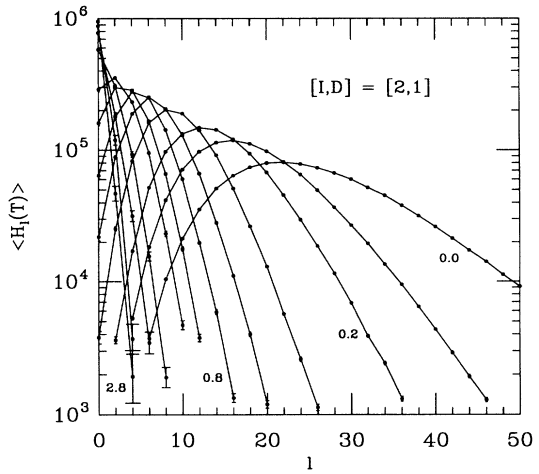

FIG. 13. Bridge of histograms: estimates of expected bar heights $\langle H_l(T)\rangle$, against energy level l, at 12 different inverse temperatures $1/T$ (see Sec. VII F), with $[I, D] = [2, 1]$. Lines join estimate that correspond to the same $1/T$ (the sum of the best values along each line equals $P = 10^6$). Selected lines are labeled by the values of $1/T$ to which they correspond. An error bar (the random error) accompanies each estimate, though only the largest error bars (note the logarithmic scale) are discernible. The line of estimates for $1/T = 0.0$ is proportional to the density of states.

(TMC 5) Finally, an estimate of $\ln[\mathcal{N}_r(I,D)/\mathcal{N}_S(I,D)]$ is calculated from the bridge of histograms (i.e., from estimates of expected bar heights) by way of the histogram method (viz., Ferrenberg and Swendsen's prescription—see Ref. 67, extended to include l-dependent autocorrelation functions—see Sec. VII B).

Sundry details: In stage (TMC 3), the use of a memory loop and the spacing of the time displacements ($\tau = 2^q$) at which best values for normalized autocorrelation functions are calculated together lead to a quick, yet robust, yet memory-efficient way to find autocorrelation times. The straight-line fit whereby the best value of the autocorrelation time $\tau_l^{\rm corr}$ is calculated uses only those $(\langle c_l[e(\tau)]c_l[e(0)]\rangle_{\rm norm})_{\rm BV}$ greater than $\exp[-1] \approx 0.3679$; i.e., the fit ignores the noise floor of $(\langle c_l[e(\tau)]c_l[e(0)]\rangle_{\rm norm})_{\rm BV}$.

F. Results: entropy per unit area (estimation of s_a^r and K_ξ)

Thermal Monte Carlo runs were performed for small, yet nontrivial, inflation orders I and array dimensions D: $[I,D]$ = [1,2], [1,3], ..., [1,6], [2,1], and [2,2]. Every run had the following specifications: $Q = 18$, $P = 10^6$, $1/T = \{0.0, 0.1, 0.2, 0.4, 0.6, 0.8, 1.0, 1.2, 1.6, 2.0, 2.4, 2.8\}$. (The Monte Carlo run for $[I,D]$ = [2,2] (the longest of them) required about 46 h of computer time on an IBM RS-6000.) Regarding the error analysis of Sec. VII B, all autocorrelation functions appeared to decay exponentially. See Fig. 13 and Table II (note that the estimates of $s_a^r[I,D]$ (Table II, rightmost column) have fractional random errors that are on the order of 1×10^{-4}).

For small background phasons strains $\underline{B}$ that take the form of Eq. (19), the entropy per unit area, in the thermodynamic limit $L \to \infty$, should obey Eq. (22) with $\underline{\tilde{E}} = 0$:

$$\omega[0] = s_a^r - \tfrac{1}{2}K_\xi B^2. \tag{89}$$

The authors hypothesize the following *ad hoc* finite-size (both finite-L and finite-B) scaling form for the entropy per unit area of a maximally random ensemble that comprises every $[I,D]$-type approximant:

$$S^r[I,D]/L^2 \equiv s_a^r[I,D] = s_a^r - \tfrac{1}{2}K_\xi B^2 + A[I]/L^2, \tag{90}$$

where B (dependent on I, but independent of D) is given by Eq. (47), $A[I]$ (dependent I, but independent of D) is an unknown parameter, and L (dependent on both I and D) is given by Eq. (45); for the purposes of finite-size scaling, the reader should regard $s_a^r[I,D]$ as a function of L and B, with unknown parameters s_a^r, K_ξ, and $A[I]$. Because $[I,D]$-type approximants satisfy periodic (toroidal) boundary conditions, a $1/L$ term should not be needed on the right-hand side of Eq. (90)—see Ref. 47. Figure 14 displays, against $1/L^2$, the estimates of $s_a^r[I,D]$ that appear in the rightmost column of Table II, which were elicited from the thermal Monte Carlo runs that are described above. Note that systematic (finite-L and finite-B) effects are much larger than the error bars. The author's finite-size scaling procedure, whereby estimates of s_a^r (s_v^r) and K_ξ were obtained, consisted of three parts.

(i) A straight-line least-squares fit to the best values of $s_a^r[1,D]$, against $1/L^2$, for $D = 3$, 4, 5, and 6 (y (no error bars) $= u + vx$, where $y = s_a^r[1,D]$, $u = s_a^r[1,\infty]$, $v = A[1]$, and $x = 1/L^2$); the intercept at $1/L^2 = 0$ gave an estimate (best value ± random error) of $s_a^r[1,\infty] = (s_a^r - \frac{1}{2}K_\xi B^2)$, with $B = \lambda^{-2}$.

(ii) A straight-line least-squares fit to the best values of $s_a^r[2,D]$, against $1/L^2$, for $D = 1$ and 2 (y (no error bars) $= u + vx$, where $y = s_a^r[2,D]$, $u = s_a^r[2,\infty]$, $v = A[2]$, and $x = 1/L^2$); the intercept at $1/L^2 = 0$ gave a best value [but no random error—there were as many free parameters (u and v) as data points ($D = 1$ and 2); see Fig. 14] for $s_a^r[2,\infty] = (s_a^r - \frac{1}{2}K_\xi B^2)$, with $B = \lambda^{-4}$; an estimate of $s_a^r[2,\infty]$ was then cobbled together out of this best value and—for want of something better—the random error of the estimate that was obtained in part (i) above.

(iii) A straight-line least-squares fit to the (two) estimates of $s_a^r[I,\infty]$ (one for $I = 1$, the other for $I = 2$) that were obtained from parts (i) and (ii) above (see Fig. 15; y (with error bars) $= u + vx$, where $y = s_a^r[I,\infty]$, $u = s_a^r$, $v = K_\xi$, and $x = \frac{1}{2}B^2$) gave estimates of both s_a^r (the intercept at $\frac{1}{2}B^2 = 0$) and K_ξ ($-1 \times$ the slope):

$$s_a^r = 0.13137 \pm 0.00044 \tag{91}$$

TABLE II. Results of thermal Monte Carlo runs: I is the inflation order; D is the array dimension; $\ln[\mathcal{N}_r(I,D)/\mathcal{N}_S(I,D)]$ is the entropy change between $T = 0$ and $T = \infty$ (see Sec. VII C, fourth paragraph); $S^S[I,D] = \ln[\mathcal{N}_S(I,D)]$ is the entropy at $T = 0$, i.e., the entropy of the subensemble that comprises Stampfli tilings; L^2 is the area of the (square) $[I,D]$-type unit cell [see Eq. (45)]; recall that $\lambda = (2+\sqrt{3})$; $s_a^r[I,D] = S^r[I,D]/L^2 = \ln[\mathcal{N}_r(I,D)]/L^2$ is the entropy per unit area of the maximally random ensemble that comprises every $[I,D]$-type square-triangle approximant.

$[I,D]$	Estimate of $\ln[\mathcal{N}_r(I,D)/\mathcal{N}_S(I,D)]$	$S^S[I,D]$	L^2	Estimate of $s_a^r[I,D]$
[1,2]	4.2595 ± 0.0026	4 ln[2]	$4\lambda^2$	0.126220 ± 0.000046
[1,3]	10.051 ± 0.013	9 ln[2]	$9\lambda^2$	0.129950 ± 0.000100
[1,4]	17.861 ± 0.020	16 ln[2]	$16\lambda^2$	0.129917 ± 0.000090
[1,5]	27.538 ± 0.023	25 ln[2]	$25\lambda^2$	0.128852 ± 0.000065
[1,6]	39.669 ± 0.031	36 ln[2]	$36\lambda^2$	0.128880 ± 0.000061
[2,1]	11.683 ± 0.013	16 ln[2]	λ^4	0.117389 ± 0.000069
[2,2]	54.860 ± 0.142	64 ln[2]	$4\lambda^4$	0.127865 ± 0.000184

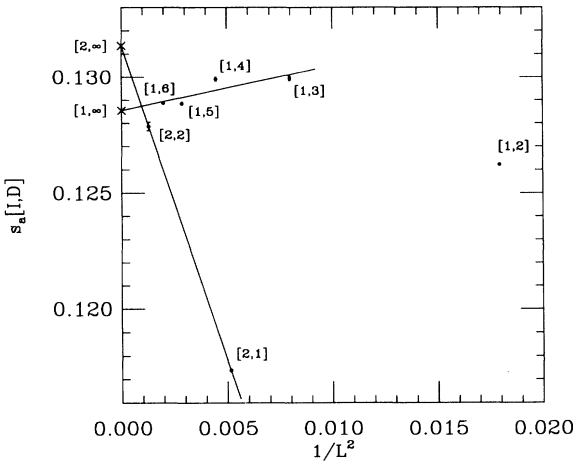

FIG. 14. Finite-size scaling: estimates of entropy per unit area $s_a[I,D]$, each labeled by $[I,D]$, against inverse unit-cell area $1/L^2$. Note that the entropy per unit area for $I=1$ does not vary monotonically with D. The two straight lines and their intercepts (crosses) at $1/L^2=0$ represent parts (i) and (ii) of the *ad hoc* finite-size scaling procedure (see Sec. VII F).

and

$$K_\xi = 1.09 \pm 0.24. \tag{92}$$

The estimates (65) and (92) thankfully satisfy inequalities (16) and (17), by comfortable margins (the latter inequality is a nontrivial consistency check). At zero phason strain, the number of vertices per unit area equals

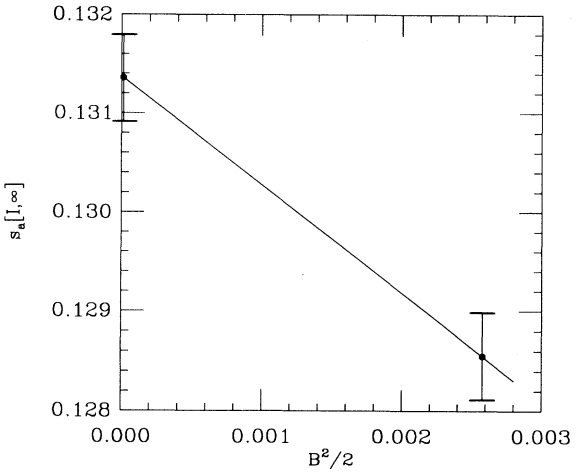

FIG. 15. Estimation of the entropy per unit area at zero phason strain s_a^r and the second-order elastic constant K_ξ: best values for the entropy per unit area at infinite array dimension $s_a^r[I,\infty]$, against $\frac{1}{2}B^2$ [see Eq. (19)]. The rightmost estimate corresponds to $B=1/\lambda^2$. The leftmost estimate, which lies close to (but not on) the ordinate, corresponds to $B=1/\lambda^4$. The straight line represents part (iii) of the *ad hoc* finite-size scaling procedure (see Sec. VII F), whereby the estimates of s_a^r, K_ξ, and s_v^r that Eqs. (91)–(93) display were obtained.

$(\frac{1}{2}+\frac{1}{\sqrt{3}})$ [see Eqs. (48)–(50)]. An estimate of the entropy per vertex at zero phason strain, the equivalent of Eq. (91), is thus

$$s_v^r = 0.12194 \pm 0.00041. \tag{93}$$

The authors stress that the above finite-size scaling analysis [i.e., Eq. (90) and parts (i)–(iii) above] is tenuous. The systematic errors that hide in the best values of s_a^r, K_ξ, and s_v^r [Eqs. (91)–(93)] are probably several times larger than the random errors quoted. By way of a transfer-matrix method, Kawamura[40] estimated the entropy per vertex at zero phason strain s_v^r to be 0.119 ± 0.001. By way of a (numerical) Bethe-ansatz method, Widom[41,42] recently obtained a superb estimate of the entropy per unit area at zero phason strain s_a^r and an accurate estimate of the second-order elastic constant K_ξ: $s_a^r = 0.129341553 \pm 0.000000002$, which is equivalent to $s_v^r = 0.120055247 \pm 0.000000002$, and $K_\xi = 1.43008 \pm 0.00004$. The discrepancy (roughly five standard deviations) between the authors' estimate of s_a^r [Eq. (91)] and Widom's (independent) estimate of the same quantity indicates that systematic errors lurk in the above, *ad hoc*, finite-size scaling analysis. The authors reckon that their estimate would agree much better with Widom's estimate if they had been able to obtain estimates of $s_a^r[2,D]$ for $D>2$ (the straight line in Fig. 14 that joins the best value of $s_a^r[2,1]$ to the best value of $s_a^r[2,2]$ probably overshoots $s_a^r[2,\infty]$). Concerning the question as to whether or not the zipper update move connects arbitrary square-triangle tilings (see Sec. IV), the authors are relieved, nonetheless, to find that their estimate of s_v^r [Eq. (91)], obtained by way of the zipper update move, is not significantly lower than the (independent) estimates of s_v^r that Kawamura and Widom obtained.

VIII. TRANSFER MATRICES

Random tilings can be represented by spin configurations, whose spins lie on regular lattices. Ensembles that comprise random tilings are thus similar to certain well-studied statistical models (e.g., ice-type models[43,80]), except that their microstates satisfy more exotic constraints. To the authors' knowledge, random square-triangle tilings do not correspond to the microstates of any known "exactly solved model".[80] This section motivates and describes a transfer-matrix method for calculating the entropy per vertex of random square-triangles tilings that tile strips, whereby the entropy per unit area at zero phason strain $[s_a^r]$ and the elastic constants $[K_\xi, J,$ and—with some extra work—$K_\mu]$ can be estimated.

A. Random tilings as spin configurations

Consider an ensemble (a system[5]) comprising every tiling (either eightfold-symmetric rhombus, tenfold-symmetric rhombus, square-triangle, or whatever) that tiles a *strip*, where the longitudinal dimension (the length) of the strip is infinite, the transverse dimension

(the width) of the strip is finite, and the longitudinal axis of the strip runs parallel to a symmetry direction. Next, consider a regular, square spin lattice, whose (discrete) dimensions are $[L \times \infty]$ and whose spins are all q state (both L and q are finite, positive integers). Now, suppose that a one-to-one map exists between the members of the above ensemble and certain configurations of the spin lattice; the entropy per vertex of the ensemble can then be found by way of a transfer-matrix calculation. To facilitate the rest of this section, some jargon is defined forthwith: Any map of the above variety is a *transfer-matrix* map; a tiling that tiles the strip is a *stack* of *layers*; the spin lattice is a stack of *rows* (each row contains L spins); an *allowed* spin configuration corresponds to a tiling that tiles the strip (not all spin configurations are allowed); the number of vertices per row of the lattice, for tilings that tile the strip, equals V.

Transfer-matrix maps are known[81] for both eightfold-symmetric[82] and tenfold-symmetric[3,83] (random) rhombus tilings. To estimate the entropy per vertex at zero background phason strain, the transfer matrices that correspond to these particular maps require chemical potentials; in other words, grand canonical ensembles of spin configurations have to be invoked.[84] Some time ago, Kawamura[85] discovered a transfer-matrix map for (random) square-triangle tilings, for which $q = 8$, L is an arbitrary positive integer, the longitudinal axis of the strip is parallel to $(\cos[\alpha j], \sin[\alpha j])^{\parallel}$ (j is an integer), and "exceptional configurations" must be excluded. Kawamura[40] recently used this map to estimate s_v^r, the entropy per vertex of infinite random square-triangle tiling at zero background phason strain. The transfer matrices that Kawamura constructed, however, were extremely sparse. With a modern computer, he could only calculate the entropy per vertex for $L \leq 10$. Nonetheless, Kawamura managed to obtain a good estimate of s_v^r [viz., $s_v^r = 0.119 \pm 0.001$], though his data severely tested the finite-L scaling form that he used. A different, more efficient[86] transfer-matrix map for square-triangle tilings is presented in what follows.

B. Transfer-matrix map for square-triangle tilings

In contrast to Kawamura's map, the longitudinal axis of the strip is parallel to $(\cos[\alpha(j+\frac{1}{2})], \sin[\alpha(j+\frac{1}{2})])^{\parallel}$ (j is an integer), i.e., parallel to a direction that runs halfway between two consecutive parallel-space basis vectors. The spins used are only three-state: either "+," "−," or "0." The 0 spins of any row must occur in "00" pairs. Assume, henceforth, that the numbers of + and − spins in any row are equal; this constraint excludes spiral boundary conditions and forces (in the absence of chemical potentials) reflection symmetry in the longitudinal axis. The transfer-matrix map is defined through an example: See Figs. 16(a) and 16(b).

Now consider an $[L \times \infty]$ spin lattice (three-state spins), whose allowed spin configurations represent, under the above map, random square-triangle tilings that tile a strip of width W; periodic boundary conditions exist across the sides of the strip; every allowed spin configuration satisfies periodic boundary conditions across the ends of rows; each row contains N_{00} 00 pairs, $N_{+/-}$ + spins, and $N_{+/-}$ − spins; $L = 2(N_{00}+N_{+/-})$; V (the number of vertices per row of the lattice) $= N_{00}+2N_{+/-}$. Now suppose that a particular sequence of + spins, − spins, and 00 pairs, which defines a particular row state,[87] occupies a row of the spin lattice. Call this the *old* sequence. The rule whereby a *new* sequence of + spins, − spins, and 00 pairs can be built and/or generated on top of the old sequence is as follows: First, place a mark between the 0 spins of every 00 pair in the old sequence. Call the spins that lie between a pair of consecutive marks a *subsequence*. For each subsequence, place an 00 pair above either a possible 0− pair at the left end of the subsequence, a +− pair somewhere in the middle of the subsequence, or a possible +0 pair at the right end of the subsequence. Where possible, place a + spin above the 0 spin at the left end of each subsequence and a − spin above the 0 spin at the right end of each subsequence. Finally, fill in the gaps that remain in the new sequence by duplicating the corresponding sections of the old sequence. (The above prescription is analogous to the "SS" rule in the transfer-matrix map for tenfold-symmetric rhombus tilings—see Refs. 3 and 88.) Imagine the row-to-row transfer matrix for the (allowed) spin configurations that the above rule generates; the matrix element $T_{\alpha\beta}$ equals unity if a sequence that represents row state α can be built on top of a sequence that represents row state β; else it equals zero.

The perp.-space description of the square-triangle tilings that tile strips running parallel to $(\cos[\alpha(j+\frac{1}{2})], \sin[\alpha(j+\frac{1}{2})])^{\parallel}$ is facilitated by the use of rotated parallel-space and perp.-space Cartesian bases, $\mathbf{r} = (r_t, r_l)^{\parallel}$ and $\mathbf{f} = (f_t, f_l)^{\perp}$, where the suffixes "$t$" and "$l$" label transverse and longitudinal components, respec-

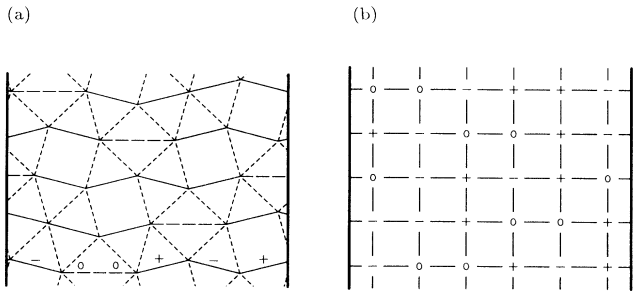

FIG. 16. The (transfer-matrix) map: (a) layers of a square-triangle tiling that tiles a strip and (b) the row-states that correspond to these layers. Periodic boundary conditions exist [in (a)] across the sides of the strip and [in (b)] across the ends of rows (both thick solid lines). Closed paths in (a), comprising the tile edges that are shared between layers (thin solid lines) and the horizontal diagonals across squares (thin long-dashed lines), correspond to rows in (b). [Edges in (a) that are not shared between layers are drawn as thin, short-dashed lines.] The tile edges (and the diagonal) along the bottommost path in (a) are decorated with the spin states to which they correspond. The catenation of these spin states forms the bottommost row state in (b).

tively. Using these Cartesian bases, the background phason strain can be decomposed as

$$\underline{B} = \begin{bmatrix} B_{tt}, & B_{tl} \\ B_{lt}, & B_{ll} \end{bmatrix}. \tag{94}$$

Now, because the numbers of + and − spins in any row are equal, $B_{tt} = 0$. In general, both B_{tl} and B_{ll} could be calculated from the left and right eigenvectors that correspond to the largest eigenvalue of the transfer matrix. Because a reflection through the longitudinal axis of the strip is a symmetry operation, however, $B_{ll} = 0$. Furthermore, because of the irrotational property of square-triangle tilings (see Sec. II B), $B_{tl} = B_{lt} \equiv B'$. Thus, in contrast to the transfer-matrix maps for both eightfold-symmetric and tenfold-symmetric (random) rhombus tilings,[3,83,84,88] every component of the background phason strain that is not automatically zero is fixed by the (periodic) transverse boundary conditions alone.[89] Note that W and B' are analogous to L and B, respectively [see Eqs. (45) and (47)]. For any finite W, B' is nonzero.

C. Small, hand-built transfer matrix

The authors constructed, by hand, the transfer matrix for the transverse boundary conditions that correspond to $N_{oo} = 1$, $N_{+/-} = 3$, $L = 8$, $V = 7$, $W = 6\cos[\pi/12] + 2\cos[\pi/4] \approx 7.20977$, and

$$B' = (3\sin[\pi/12] - \sin[\pi/4])/(3\cos[\pi/12] + \cos[\pi/4]) \approx 0.01924. \tag{95}$$

By identifying all of the row states that are related by symmetry (translations and reflections through the longitudinal axis), the transfer matrix is only 14×14. As yet another idiosyncrasy of square-triangle tilings, the 14×14 transfer matrix has a cyclical property: When raised to the fourth power it becomes block diagonal; its largest eigenvalue $\Lambda_{\max}$ can be found by solving just a quadratic equation, whose largest root equals $\Lambda_{\max}^4$; in effect, the transfer matrix is just 2×2. The resultant entropy per vertex is

$$s_1 = \frac{\Lambda_{\max}}{V} = \frac{\ln(12 + 16\sqrt{2})}{28} \approx 0.12659. \tag{96}$$

In comparison, the transfer matrix for $L = 10$ that Kawamura[40] constructed is 199296×199296; the resultant entropy per vertex is $s_2 \approx 0.20970$. Now, Widom[41,42] recently estimated the entropy per vertex of (infinite) random square triangles at zero phason strain to be $s_v^r = 0.120055247 \pm 0.000000002$. Compared to the value of s_2, the value of s_1 lies remarkably close to s_v^r (i.e., Widom's estimate). Why should the "2×2" transfer matrix give an entropy per vertex (s_1) that is so much closer to s_v^r than the entropy per vertex (s_2) that the "199296×199296" transfer matrix gives? The following reasons can be put forward.

(i) Because the transfer-matrix map incorporates transverse boundary conditions that are periodic, (a) row states related by translational symmetry can be identified, thereby reducing the dimension of each transfer matrix by a factor of L; (b) edge-surface effects, which would scale as $1/L$, are absent (the leading finite-L effects thus ought to scale as $1/L^2$—see Ref. 47); (c) each transfer matrix block diagonalizes when raised to a certain power [this (cyclical) property is related to the existence of domain walls (see below)], and as a result, the effective dimension of each transfer matrix is reduced by (another) factor of order L. In contrast, the transfer matrices that Kawamura constructed assume free transverse boundary conditions; as a result, their dimensions are huge, even for modest L, and finite-L effects arise that scale as $1/L$.

(ii) The (periodic) transverse boundary conditions that correspond to the 2×2 transfer matrix engender a weak background phason strain: The value of B' [Eq. (95)] is small. As a result, the systematic error due to the finiteness of B' ought to be small. [Note that the entropy per unit area, as a function of B', varies quadratically, not linearly, near $B' = 0$. Given Eqs. (50), (89), and (92), the systematic error should equal $-K_\xi B'^2/(2v_a) \approx -1.6 \times 10^{-4}$.]

Despite appearances, the above prescription for constructing transfer matrices (Sec. VIII B) is quite simple: Because the numbers of + and − spins in a row are conserved from one row to the next, the + and − spins in consecutive rows can be regarded as positive and negative *domain walls*[82] or, equivalently, as the trajectories of left-moving and right-moving particles that interact. Viewed as domain walls and/or trajectories, random square-triangle tilings are reminiscent of the (exactly solved) square-ice model.[43,80] Widom[41,42] has fruitfully pursued this analogy.

IX. CONCLUSION

A. Summary of results

A summary of the analytical results that this paper contains is as follows.

(i) The representative surface of any square-triangle tiling is irrotational; it can thus be expressed as the gradient of a scalar potential (Sec. II B).

(ii) Maximally random ensembles that comprise (random) square-triangle tilings are described by an entropy density (Secs. III A and III B), which is derived up to third order in the phason strain (Appendix A). The effect that a small, fourfold-symmetric background phason strain has on the magnitudes of phason-mode fluctuations is calculated to first order in the background phason strain, by way of a Legendre transformation (Secs. III C–III F).

(iii) An update move is formulated that effects a zipper of squares and triangles (Sec. IV, Fig. 3). Athermal and thermal Monte Carlo steps are constructed around this update move (Secs. VI A and VII D), which satisfy detailed balance for maximally random and canonical ensembles of square-triangle tilings, respectively (Appendix B).

(iv) The entropy per unit area of (random) Stampfli tilings at zero phason strain (i.e., 12-fold symmetry) is computed via recursion (Sec. V B).

(v) Various Monte Carlo methods for estimating the total entropies of maximally random ensembles are described, and their relative merits discussed. Some conceptual insight is given as to why the Ferrenberg-Swendsen histogram method is more efficient at estimating total entropies than the alternative thermal Monte Carlo methods. The histogram method is extended to cope with autocorrelation times that depend on energy level (Secs. VII A and VII B, and Appendix C).

(vi) A pseudo-Hamiltonian is constructed, which defines canonical ensembles of random square-triangle tilings. The (degenerate) ground states of such ensembles comprise Stampfli tilings. The excited states have energies that occupy discrete energy levels, which are equally spaced above the ground-state energy. The degeneracy of the Stampfli tilings that compose a ground state is proven by using the parallel-axis theorem of elementary mechanics (Sec. VII C).

(vii) A map between random square-triangle tilings and certain configurations of regular, square spin lattices is presented (Sec. VIII B, Fig. 16). Using this map, an efficient transfer-matrix method for calculating the entropy per unit area of random square-triangle tilings (at various background phason strains) is formulated; the transfer matrices that are involved exhibit an unusual cyclical property (Secs. VIII B and VIII C).

Table III supplies a summary of the numerical results that this paper contains.

The reader should note that the Monte Carlo methods described in this paper complement, to some extent, the (highly efficient) Bethe-ansatz method that Widom has recently implemented: Both a good estimate of the second-order elastic constant K_μ [Eq. (65)] and a good estimate of the third-order elastic constant J [Eq. (67)] can be obtained by measuring phason-mode fluctuations (that is, by implementing the athermal Monte Carlo method that is described in Sec. VI). A reasonable estimate of the entropy per unit area s_a^r [Eq. (91)], but only a crude estimate of the second-order elastic constant K_ξ [Eq. (92)], can be obtained by invoking a pseudo-Hamiltonian and constructing energy histograms (that is, by implementing the thermal Monte Carlo method that is described in Secs. VII B–VII F). Widom, on the other hand, can obtain (see Ref. 90) a superb estimate of s_a^r and an accurate estimate of K_ξ, but he cannot obtain an accurate estimate of J; nor can he yet obtain an estimate of K_μ [this requires calculating the entropy per unit area of systems (strips) that contain unequal numbers of positive and negative domain walls].

B. Speculations and open questions

The work presented in this paper demonstrates that Monte Carlo methods can be used to estimate the parameters that describe the statistical behavior of random tilings (viz., the entropy per unit area and the elastic constants), even if the only adequate update move is highly complex. The work warns, however, that finite-size effects can be extremely misleading; that is, they can be large, dependent on the background phason strain $\underline{B}$, and nonmonotonic as a function of the system size (viz., for square unit cells, the sidelength L). Such effects, moreover, seem particularly treacherous at small background phason strains (note that, in Table II (rightmost column) and Fig. 14, the estimate of $s_a^r[2,1]$ is much smaller than the estimate of $s_a^r[2,2]$). Indeed, the whole systematics of joint finite-L–finite-$\underline{B}$ scaling, for toroidal (as opposed to cylindrical) boundary conditions, seems poorly understood; Refs. 92–94 shine some light on this matter.

From a purist's standpoint, the most prominent question is whether or not an exact solution (analogous to Lieb's solution of the square-ice model[43]) exists for random square-triangle tilings (see Refs. 41 and 42). A less ambitious goal would be to prove the connectivity property of the zipper update move (see Sec. IV and Fig. 3; note Ref. 39). Such a proof would put the Monte Carlo methods that this paper describes on a more solid foundation and could hold some mathematical interest in its

TABLE III. Summary of numerical results: Each estimate is quoted as a best value plus or minus a random error [the precise definition and meaning of each random error is given through the relevant subsection (wherein the fitting procedure is described) and/or through the relevant figure (wherein error bars are shown); the quantity Γ is introduced in Sec. VI D; the quantities s_a^r, K_μ, K_ξ, and J, are introduced in Sec. III B; $s_a^r = (\frac{1}{2} + \frac{1}{\sqrt{3}})s_v^r$—see Eq. (50); Secs. VI F and VI G detail how the estimate of Γ [Eq. (66)], the estimate of K_μ [Eq. (65)], and the estimate of J [Eq. (67)] were obtained; Sec. VII F details how the estimate of s_a^r [Eq. (91)], the (equivalent) estimate of s_v^r [Eq. (93)], and the estimate of K_ξ [Eq. (92)] were obtained; in the light of Widom's recent work (Ref. 41), the authors suspect that the best values quoted for s_a^r, s_v^r, and K_ξ hide systematic errors that are sizable, vis-à-vis the random errors quoted.

Name	Notation	Estimate
athermal Monte Carlo rate constant	Γ	0.0272 ± 0.0010
second-order ("phason-fluctuation") elastic constant	K_μ	0.4602 ± 0.0024
third-order elastic constant	J	-0.987 ± 0.022
entropy per unit area at zero phason strain	s_a^r	0.13137 ± 0.00044
entropy per vertex at zero phason strain	s_v^r	0.12194 ± 0.00041
second-order ("total-divergence") elastic constant	K_ξ	1.09 ± 0.24

own right. The dynamics of the thermal (as opposed to the athermal) Monte Carlo step (Sec. VII D), that is, how the mean zipper length depends on the temperature T and how the autocorrelation time $\tau_l^{\rm corr}$ [see Eq. (78)] depends on both T and the energy level l, was not explored. The authors do not understand why an "entropy ceiling" besets their implementation of Ma's coincidence-counting method for random square-triangle tilings (see Appendix C).

C. Physical systems

An important issue, which has received little attention to date, concerns the dynamics of real quasicrystals: Are update moves merely technical devices, or do they, in some way, mirror actual atomic rearrangements? If so, do the atoms in a (random) quasicrystal rearrange themselves in a way that resembles a flip update move, or do they rearrange themselves in a way that resembles a zipper update move? If the latter, what is the atomic equivalent of a defect tile (viz., for random square-triangle tilings, a thin (30°) rhombus or, for random canonical-cell tilings, a hexagonal bipyramid[17])? How much energy would it cost to create such an atomic defect?

Certain alloys of Ni-Cr and V-Ni/V-Ni-Si have been studied (Refs. 95 and 96 and Ref. 97, respectively), whose electronic and optical diffraction patterns exhibit 12-fold orientational symmetry and whose high-resolution electron-microscope images show bright dots that are located on the vertices of square-triangle tilings [these two relative clauses explain, to some extent, the title of this paper; the authors felt that they were obliged to include the words "12-fold-symmetric" and "quasicrystal(s)" somewhere in the title]. Contrast simulations of such images[98] appear to support an atomic model that decorates squares and triangles in a way inspired by the known atomic structures of Frank-Kasper phases.[99,100] Thus, the work presented in this paper should be relevant to three-dimensional atomic models of the above alloys that involve random square-triangle tilings that are stacked randomly;[2] the value of the entropy per unit area at zero phason strain s_a^r and the values of the elastic constants K_μ, K_ξ, and J would go some way towards predicting both the stability of such models and the sharpness of their diffraction peaks. Unlike for icosahedral or decagonal quasicrystals, all of the high-resolution electron-microscope images that have been published to date (Refs. 95–97) show either small (about 10 nm in diameter) particles or regions that coexist with the so-called σ phase. Whether or not the above alloys form true (in-the-bulk) 12-fold-symmetric (random) quasicrystals is uncertain. More experiments are needed.

D. Canonical-cell tilings

What was written in the Introduction can be inverted: (random) canonical-cell tilings are analogous to (random) square-triangle tilings. The natural sequel to the work presented in this paper would be the implementation of an update move that effects a zipper of canonical cells,[17] then the sampling of ensembles that comprise random canonical-cell approximants (whereby the elastic constants and the entropy per unit area at zero phason strain could be estimated) using Monte Carlo steps based on this update move. But an obstacle presently exists in such a scheme: Neither an acceptance region nor—unlike square-triangle tilings—an inflation rule is known for canonical-cell tilings; as a result, canonical-cell approximants that correspond to small background phason strains cannot be built easily. Recent work has, however, alleviated this problem: (i) Newman and Henley[62] have found "5/3" canonical-cell approximants [135–138 vertices ("nodes") per unit cell] by constructing a transfer matrix for the growth of canonical-cell tilings between *dead surfaces*. (ii) Mihalkovič and Mrafko[101] have built canonical-cell approximants [up to 13/8 (2464 nodes per unit cell)] through the simulated annealing of a lattice gas resident on the vertices of three-dimensional Penrose approximants (the occupied vertices of ground-state configurations correspond to the nodes of canonical-cell approximants). Thus, starting configurations (requisite for Monte Carlo runs) with sufficiently small background phason strains are now available.

ACKNOWLEDGMENTS

The authors are both grateful to Mike Widom, with whom they had many helpful discussions. For comments on the manuscript, their thanks go to him and also to Eric Cockayne, Jan von Delft, Veit Elser, Mark Newman, Rob Phillips, Alice Sheppard, and Chen Zeng. The first author (M.O.) is grateful to Mark Holzer for pointing out a serious conceptual error concerning detailed balance and to Robert Swendsen for suggesting the histogram method; he would also like to thank David Rabson and Arthur Smith for their invaluable help regarding computational matters. This work was supported by the Materials Science Center at Cornell University, under Grant No. DMR-8818558, and by the DOE, under Grant No. DE-FG02-89ER-45405.

APPENDIX A: INVARIANTS

In what follows, the general forms for $\sigma_2[\underline{E}]$ and $\sigma_3[\underline{E}]$, i.e., Eqs. (14) and (15), respectively, are derived. To avoid unnecessary formalism, the universal tools for the analysis of group representations (character tables, etc.) are not used explicitly.

First, the following complex objects ($i \equiv \sqrt{-1}$) are introduced:

$$r_\pm = r_1 \pm i r_2, \tag{A1}$$

$$h_\pm = h_1 \pm i h_2, \tag{A2}$$

$$\partial_\pm = \tfrac{\partial}{\partial r_1} \pm i \tfrac{\partial}{\partial r_2}; \tag{A3}$$

recall that $\mathbf{r} = (r_1, r_2)^{\parallel}$ and $\mathbf{h} = (h_1, h_2)^{\perp}$ (the $\mathbf{r}$ de-

pendence of **h** is implicit). Among other operations, the 12-fold symmetry group, contains rotations by $m\alpha$ radians about the origin, where m is an integer and $\alpha = \pi/6$. (For a complete list of the operations that compose the 12-fold symmetry group, see Ref. 24.) Under such rotations,

$$r_\pm \to \exp[\pm i\alpha m] r_\pm, \tag{A4}$$
$$h_\pm \to \exp[\pm i7\alpha m] h_\pm, \tag{A5}$$
$$\partial_\pm \to \exp[\pm i\alpha m] \partial_\pm. \tag{A6}$$

Translating (A4)–(A6) into words: $r_\pm$, $h_\pm$, and $\partial_\pm$ are spin ±1, spin ±7, and spin ±1 objects, respectively. A *product* of objects, whose total spin equals S_T, is a spin S object, where $S = \mathrm{mod}_{12}[S_T]$. The general form for $\sigma_n[\underline{E}]$ contains the real and imaginary parts of products, where each product is both [condition (i)] n linear in objects of the form $(\partial_\pm h_\pm)$ and [condition (ii)] invariant under rotations by $m\alpha$ radians about the origin (i.e., spin 0), and where each real-imaginary part is [condition (iii)] invariant under all of the other operations that the 12-fold symmetry group contains (viz., reflections about various lines of symmetry). Given every product that satisfies conditions (i) and (ii), the elicitation of the real and imaginary parts that satisfy condition (iii) is a straightforward task (for $n = 2$ and 3 at least).

The products that satisfy conditions (i) and (ii), for $n = 2$, are

$$\text{“}S = \mathrm{mod}_{12}[(+1+7)+(-1-7)] = 0\text{”} \quad \Rightarrow \quad (\partial_+ h_+)(\partial_- h_-), \tag{A7}$$
$$\text{“}S = \mathrm{mod}_{12}[(-1+7)+(+1-7)] = 0\text{”} \quad \Rightarrow \quad (\partial_- h_+)(\partial_+ h_-), \tag{A8}$$
$$\text{“}S = \mathrm{mod}_{12}[(-1+7)+(-1+7)] = 0\text{”} \quad \Rightarrow \quad (\partial_- h_+)(\partial_- h_+), \tag{A9}$$
$$\text{“}S = \mathrm{mod}_{12}[(+1-7)+(+1-7)] = 0\text{”} \quad \Rightarrow \quad (\partial_+ h_-)(\partial_+ h_-). \tag{A10}$$

Next, the real and imaginary parts of (A7)–(A10) are taken using Eqs. (A1)–(A3); this gives

$$\mathrm{Re}[(\partial_+ h_+)(\partial_- h_-)] = \left(\frac{\partial h_1}{\partial r_1} - \frac{\partial h_2}{\partial r_2}\right)^2 + \left(\frac{\partial h_1}{\partial r_2} + \frac{\partial h_2}{\partial r_1}\right)^2, \tag{A11}$$

$$\mathrm{Re}[(\partial_- h_+)(\partial_+ h_-)] = \left(\frac{\partial h_1}{\partial r_1} + \frac{\partial h_2}{\partial r_2}\right)^2 + \left(\frac{\partial h_1}{\partial r_2} - \frac{\partial h_2}{\partial r_1}\right)^2, \tag{A12}$$

$$\begin{aligned}\mathrm{Re}[(\partial_- h_+)(\partial_- h_+)] &= \mathrm{Re}[(\partial_+ h_-)(\partial_+ h_-)] \\ &= \left(\frac{\partial h_1}{\partial r_1} + \frac{\partial h_2}{\partial r_2}\right)^2 - \left(\frac{\partial h_1}{\partial r_2} - \frac{\partial h_2}{\partial r_1}\right)^2,\end{aligned} \tag{A13}$$

$$\begin{aligned}\mathrm{Im}[(\partial_+ h_+)(\partial_- h_-)] &= -\mathrm{Im}[(\partial_- h_+)(\partial_+ h_-)] \\ &= 0,\end{aligned} \tag{A14}$$

$$\begin{aligned}\mathrm{Im}[(\partial_- h_+)(\partial_- h_+)] &= -\mathrm{Im}[(\partial_+ h_-)(\partial_+ h_-)] \\ &= -2\left(\frac{\partial h_1}{\partial r_1} + \frac{\partial h_2}{\partial r_2}\right)\left(\frac{\partial h_1}{\partial r_2} - \frac{\partial h_2}{\partial r_1}\right).\end{aligned} \tag{A15}$$

Now, (A15) fails condition (iii); (A11)–(A13), on the other hand, are invariant under every operation that the 12-fold symmetry group contains. Any linear combination of invariants is also invariant; (A11)–(A13) can thus be replaced by

$$\text{“[(A12) + (A13)]/2”} = \left(\frac{\partial h_1}{\partial r_1} + \frac{\partial h_2}{\partial r_2}\right)^2, \tag{A16}$$

$$\text{“[(A12) − (A13)]/2”} = \left(\frac{\partial h_1}{\partial r_2} - \frac{\partial h_2}{\partial r_1}\right)^2, \tag{A17}$$

$$\text{“[(A11) − (A16) − (A17)]/4”} = \left(\frac{\partial h_1}{\partial r_2}\frac{\partial h_2}{\partial r_1} - \frac{\partial h_1}{\partial r_1}\frac{\partial h_2}{\partial r_2}\right). \tag{A18}$$

Recall Eq. (10); the factors (A16), (A17), and (A18) multiply the constants $-\frac{1}{2}K_\mu$, $-\frac{1}{2}K_\nu$, and $-\frac{1}{2}K_\xi$, respectively, in Eq. (14). Note that the irrotational property [Eq. (11)] reduces the number of second-order elastic constants from 3 to 2; that is, the factor (A17) vanishes for square-triangle tilings.

The only products that satisfy conditions (i) and (ii), for $n = 3$, are

$$\text{“}S = \mathrm{mod}_{12}[3\times(+1+7)] = 0\text{”} \quad \Rightarrow \quad (\partial_+ h_+)^3, \tag{A19}$$
$$\text{“}S = \mathrm{mod}_{12}[3\times(-1-7)] = 0\text{”} \quad \Rightarrow \quad (\partial_- h_-)^3. \tag{A20}$$

Next, the real and imaginary parts of (A19) and (A20) are taken; this gives

$$\begin{aligned}\mathrm{Re}[(\partial_+ h_+)^3] &= \mathrm{Re}[(\partial_- h_-)^3] \\ &= \left(\frac{\partial h_1}{\partial r_1} - \frac{\partial h_2}{\partial r_2}\right)\left\{\left(\frac{\partial h_1}{\partial r_1} - \frac{\partial h_2}{\partial r_2}\right)^2 - 3\left(\frac{\partial h_1}{\partial r_2} + \frac{\partial h_2}{\partial r_1}\right)^2\right\},\end{aligned} \tag{A21}$$

$$\begin{aligned}\mathrm{Im}[(\partial_+ h_+)^3] &= -\mathrm{Im}[(\partial_- h_-)^3] \\ &= \left(\frac{\partial h_1}{\partial r_2} + \frac{\partial h_2}{\partial r_1}\right)\left\{3\left(\frac{\partial h_1}{\partial r_1} - \frac{\partial h_2}{\partial r_2}\right)^2 - \left(\frac{\partial h_1}{\partial r_2} + \frac{\partial h_2}{\partial r_1}\right)^2\right\}.\end{aligned} \tag{A22}$$

Condition (iii) excludes (A22); only (A21) is invariant under every operation that the 12-fold symmetry group contains. The factor (A21) multiplies the constant $-\frac{1}{6}J$ in Eq. (15).

APPENDIX B: DETAILED BALANCE

Because the zipper update move is so complex, detailed balance is a nontrivial issue. A joint proof of detailed balance for the athermal Monte Carlo step (Sec. VI A)

and the thermal Monte Carlo step (Sec. VII D) is given in what follows.

The zipper update move effects a zipper of squares and triangles, where the zipper is chosen in a random fashion. A *realization* of the zipper update move involves a creation, a sequence of submoves, and an annihilation (see Sec. IV and Fig. 4). The probability of a particular realization $\mathcal{R}$, which changes the original (see Sec. VI A) square-triangle tiling $\mathcal{T}$ into a trial square-triangle tiling $\mathcal{T}'$, is given by

$$P[\mathcal{R}] = 1/N_h \times 1/2 \times (1/2)^{N_B(\mathcal{R})}, \tag{B1}$$

where N_h is the number of regions that comprise an adjoining square and triangle that are present in $\mathcal{T}$, and $N_B(\mathcal{R})$ is the number of B-type flips that $\mathcal{R}$ executes. The factors that appear on the right-hand side of Eq. (B1) are derived from the inner workings of the zipper update move (see Fig. 4); from left to right, their origins are as follows: When a pair of thin rhombi are created, one out of the N_h regions that comprise an adjoining square and triangle that $\mathcal{T}$ contains is chosen at random; one of these two thin rhombi is chosen at random to be the rhombus that moves first; with each B-type flip, one of two possible flips [see Fig. 4(c)] is chosen at random. Note that a particular realization is not equivalent to a particular zipper; different realizations effect the same zipper. With a zipper that does not self-intersect, the number of distinct realizations that rearrange the zipper equals the length of the zipper (i.e., L_Z—see Sec. VI B).

Now, the probability of the *reverse* realization $\mathcal{R}^*$, which changes the trial square-triangle tiling $\mathcal{T}'$ back into the original square-triangle tiling $\mathcal{T}$, is given by

$$P[\mathcal{R}^*] = 1/N_h' \times 1/2 \times (1/2)^{N_B(\mathcal{R}^*)}, \tag{B2}$$

where N_h' is the number of regions that comprise an adjoining square and triangle that are present in $\mathcal{T}'$, and $N_B(\mathcal{R}^*)$ is the number of B-type flips that $\mathcal{R}^*$ executes. A subtle point is that all bounces [see Fig. 4(e)] are reversible, no matter how (with regards to their relative orientation) the two thin rhombi collide. The keystone of the proof is that $N_B(\mathcal{R}^*)$ necessarily equals $N_B(\mathcal{R})$: a B-type flip in reverse is also a B-type flip.

Under an application of the athermal-thermal Monte Carlo step, the probability of going from $\mathcal{T}$ to $\mathcal{T}'$ via the realization $\mathcal{R}$ is given by

$$P[\mathcal{T} \to \mathcal{T}'; \mathcal{R}] = 1 \times P[\mathcal{R}], \tag{B3}$$

if $C \geq 1$, and by

$$P[\mathcal{T} \to \mathcal{T}'; \mathcal{R}] = C \times P[\mathcal{R}], \tag{B4}$$

if $C < 1$; the ratio C is defined by Eq. (52) for the athermal Monte Carlo step and by Eq. (88) for the thermal Monte Carlo step. Under an application of the athermal-thermal Monte Carlo step, the probability of going from $\mathcal{T}'$ to $\mathcal{T}$ via the reverse realization $\mathcal{R}^*$ is given by

$$P[\mathcal{T}' \to \mathcal{T}; \mathcal{R}^*] = (1/C) \times P[\mathcal{R}^*], \tag{B5}$$

if $C \geq 1$, and by

$$P[\mathcal{T}' \to \mathcal{T}; \mathcal{R}^*] = 1 \times P[\mathcal{R}^*], \tag{B6}$$

if $C < 1$.

Detailed balance for the athermal Monte Carlo step: by Eqs. (52) and (B1)–(B6), $P[\mathcal{T} \to \mathcal{T}'; \mathcal{R}] = P[\mathcal{T}' \to \mathcal{T}; \mathcal{R}^*]$, for any C. Because (i) realizations are disjoint and (ii) a reverse realization exists for every realization, the probability of going from $\mathcal{T}$ to $\mathcal{T}'$, via any realization, equals the probability of going from $\mathcal{T}'$ to $\mathcal{T}$, via any reverse realization, i.e.,

$$\begin{aligned} P[\mathcal{T} \to \mathcal{T}'] &= \sum_{\{\mathcal{R}\}} P[\mathcal{T} \to \mathcal{T}'; \mathcal{R}] \\ &= \sum_{\{\mathcal{R}^*\}} P[\mathcal{T}' \to \mathcal{T}; \mathcal{R}^*] = P[\mathcal{T}' \to \mathcal{T}]. \end{aligned} \tag{B7}$$

By definition, (B7) implies that the athermal Monte Carlo step satisfies detailed balance for a maximally random ensemble.

Detailed balance for the thermal Monte Carlo step: by Eqs. (88) and (B1)–(B6), $P[\mathcal{T} \to \mathcal{T}'; \mathcal{R}] = \exp[(U - U')/T] \times P[\mathcal{T}' \to \mathcal{T}; \mathcal{R}^*]$, for any C. The probability of going from $\mathcal{T}$ to $\mathcal{T}'$, via any realization, thus equals $\exp[(U - U')/T]$ times the probability of going from $\mathcal{T}'$ to $\mathcal{T}$, via any reverse realization, i.e.,

$$\begin{aligned} P[\mathcal{T} \to \mathcal{T}'] &= \sum_{\{\mathcal{R}\}} P[\mathcal{T} \to \mathcal{T}'; \mathcal{R}] \\ &= \sum_{\{\mathcal{R}^*\}} \exp[(U - U')/T] \times P[\mathcal{T}' \to \mathcal{T}; \mathcal{R}^*] \\ &= \exp[(U - U')/T] \times P[\mathcal{T}' \to \mathcal{T}]. \end{aligned} \tag{B8}$$

By definition, (B8) implies that the thermal Monte Carlo step satisfies detailed balance for a canonical ensemble at temperature T.

Note how, in both cases, detailed balance is proven realization by realization. Detailed balance for the Swendsen-Wang[44] and Wolff[45] (cluster-flip) algorithms is proven by invoking similar ideas.

APPENDIX C: MA'S COINCIDENCE-COUNTING METHOD

This appendix describes, in brief, how Ma's coincidence-counting method was implemented to estimate the total entropies of maximally random ensembles that comprise random $[I, D]$-type approximants. First, note that the entropy per unit area of random square-triangle tilings is relatively small (≈ 0.13). Ma's method should thus be able to estimate total entropies for systems whose unit cells contain hundreds of vertices. The next two paragraphs describe crucial details; the final paragraph presents and discusses results.

The zipper update move (Sec. IV) does not conserve the sum rationally related perp.-space position vector of the vertices within an $[I, D]$-type unit cell; in other words, the quantity $\sum_{n=1}^{N_v} \vec{\mathbf{f}}_{v_n} = N_v \times \langle \vec{\mathbf{f}} \rangle$ [see Eq. (84)] is not conserved. As a result, few coincidences between

approximants would occur in a sequence that were generated by the athermal Monte Carlo step (Sec. VI A) alone. [The sum rationally related perp.-space position vector would wander (a random walk) in perp. space.] The *coincidence-counting athermal Monte Carlo step* that was actually used, however, consisted of two stages: First, the athermal Monte Carlo step was applied; second, the extant approximant was translated through an integral combination of four-dimensional basis vectors (duly respecting toroidal boundary conditions), such that the sum rationally related perp.-space position vector of the translated approximant occupied one of the sites in an *irreducible* $D \times D$ square grid of sites in perp. space (this process is akin to the "gauge transformation" that Refs. 33 and 91 discuss). The latter stage had the effect of factoring out the (infinite) entropy due to the continuous degrees of freedom that are associated with overall translations in parallel space.

The four-dimensional position vectors of the vertices in each approximant were first *Shell sorted* (see Ref. 58), then *bit packed* (after bit packing, each four-dimensional position vector required only 32 bits of computer memory) into a unique *word*. The map between approximants and words was one to one; *hash clashes* (see Ref. 58) were impossible. Coincidences between approximants were recognized by spotting word repetitions; that is, pairs of words were checked for equivalence. At least 10^5 Monte Carlo steps separated the words in each pair. An efficient algorithm was used for spotting word repetitions (i.e., word-pair equivalences): A binary tree of words was first grown (a fully grown tree contained typically 10^4 words); then (after an interval during which many Monte Carlo steps were executed) word repetitions were spotted (in "logarithmic computer time") by searching through the tree (again, see Ref. 58). In effect, a great many (typically 4×10^{10}) pairs of words (each pair represented a candidate coincidence) were checked for equivalence.

The total entropies of ensembles that comprise random $[I,D]$-type approximants, viz., $S^r[I,D]$ (recall that I is the inflation order and that D is the array dimension—see Sec. V C), were thereby estimated to be

$$\begin{aligned} S^r[1,2] &= 7.02997 \pm 0.00018, \\ S^r[1,3] &= 16.241 \pm 0.017, \\ S^r[1,4] &= 17.434 \pm 0.031, \\ S^r[2,1] &= 17.389 \pm 0.031. \end{aligned} \tag{C1}$$

The estimates of entropies per unit area, viz., $s_a^r[I,D]$, that are equivalent to the above estimates of total entropies ($s_a^r[I,D] = S^r[I,D]/L^2$), are

$$\begin{aligned} s_a^r[1,2] &= 0.126182 \pm 0.000003, \\ s_a^r[1,3] &= 0.12956 \pm 0.00014, \\ s_a^r[1,4] &= 0.07823 \pm 0.00014, \\ s_a^r[2,1] &= 0.08964 \pm 0.00016. \end{aligned} \tag{C2}$$

The estimates of $s_a^r[I,D]$ for $[I,D]$ = [1,2] and [1,3] agree reasonably well with the equivalent estimates that were obtained by way of the Ferrenberg-Swendsen histogram method (see Table II, rightmost column). The above estimates of $s_a^r[I,D]$ for $[I,D]$ = [1,4] and [2,1], however, seem erroneous. The authors implementation of Ma's coincidence-counting method appeared to hit a *total-entropy ceiling* ≈ 17: With ensembles whose (true) total entropies were greater than 17 or so, too many coincidences always occurred. As a result, the total entropies of such ensembles were systematically underestimated. Why does the total-entropy ceiling exist? As regards this question, the reader should understand that (i) Ma's coincidence-counting method severely tests the implicit assumption of *ergodicity* and that (ii) the properties of connectivity and detailed balance do not specify the shape of the *coincidence autocorrelation function*. The total-entropy ceiling might exist due to a statistical (not Poincaré) recurrence phenomenon, akin to the propensity for a random walk in two dimensions to return to its starting point. Such a phenomenon would give the coincidence autocorrelation function a long-time tail, and as a result, the words that compose each pair would not be statistically independent. But this is idle speculation; the occurrence of too many coincidences remains a mystery.

---

* Present address: The Niels Bohr Institute, Blegdamsvej 17, DK-2100 Copenhagen, Denmark.

[1] A comprehensive and pedagogical review is *Quasicrystals: The State of the Art*, edited by P. J. Steinhardt and D. P. DiVincenzo (World Scientific, Singapore, 1991).

[2] C. L. Henley, in *Quasicrystals* (Ref. 1), Chap. 15, Sec. 3, explains the concept of phason strain.

[3] C. L. Henley, J. Phys. A **21**, 1649 (1988).

[4] Under a *decoration scheme*, every tile of the same type is decorated with atoms in the same way.

[5] The words *ensemble* and *system* denote the same entity, that is, a "Gibbsian ensemble." They serve, however, to distinguish between such an entity's probabilistic aspects and its physical aspects, respectively.

[6] The authors' *zipper* is named in analogy to the type of clothing fastener that is called a "zipper" (after the trademark "Zipper"), since such a fastener's configuration is changed as its slider moves along it, but is restored if the slider's motion is reversed—just as a tiling configuration is changed or restored as a defect tile moves through it.

[7] Of course, an infinite random tiling, *per se*, has no symmetry whatsoever. Were precision necessary to avoid misunderstanding, "Infinite random square-triangle tilings have ..." should be replaced by "The maximally random ensemble of infinite square-triangle tilings at zero (background) phason strain has ...." Similar alterations could be made, *mutatis mutandis*, throughout this paper.

[8] L.-H. Tang, Phys. Rev. Lett. **64**, 2390 (1990).

[9] L. J. Shaw, V. Elser, and C. L. Henley, Phys. Rev. B **43**, 3423 (1991).

[10] K. J. Strandburg, Phys. Rev. B **44**, 4644 (1991).

[11] C. L. Henley and V. Elser, Philos. Mag. B **53**, 59 (1986).

[12] M. Audier, Ch. Janot, M. de Boissieu, and B. Dubost, Philos. Mag. B **60**, 437 (1989).

[13] W. Ohashi, doctoral thesis, Harvard University, Cambridge, Massachusetts, 1989.

[14] A *good* atomic structure has a low (configuration) energy. Electronic-structure calculations usually find that

the *best* atomic structures have neither regions void of atoms nor regions where atoms lie too close together. Accurate electronic-structure calculations for the (intermetallic) alloys that form quasicrystals are difficult. As yet undiscovered, or to-date unproven, selection criteria might operate.

[15] C. L. Henley, Phys. Rev. B **43**, 993 (1991).

[16] For a more comprehensive discussion apropos the reasons that motivate the study of canonical-cell tilings, see C. L. Henley, in *Quasicrystals: Proceedings of the 12th Taniguchi Symposium*, Springer Series in Solid-State Sciences Vol. 93, edited by T. Fujiwara and T. Ogawa (Springer-Verlag, Berlin, 1990), p. 38.

[17] M. Oxborrow and C. L. Henley (unpublished). (The analog of a thin rhombus is a hexagonal bipyramid that looks somewhat like a diskus.)

[18] The meaning of the technical adjective "adequate" is defined in Sec. IV.

[19] P. Stampfli, Helv. Phys. Acta **59**, 1260 (1986).

[20] The meaning of the technical verb "to connect" is defined in Sec. IV.

[21] V. Elser, J. Phys. A **17**, 1509 (1983).

[22] The "7α" convention is taken, the same convention that Leung, Henley, and Chester (Ref. 23) took. Socolar (Ref. 24) took instead—translating into the authors' terminology—the "5α" convention (both 5 and 7 are relatively prime to 12). The transformation $f_2 \to -f_2$ relates the perp. spaces that are defined by the two conventions. With the "7α" convention, the metric of the dot product between perp. and parallel space [Eqs. (6), (23), (24), and (26) all use this dot product] has the (simple) signature $[+,+]$. (If the "5α" convention were taken, the signature would be $[+,-]$.)

[23] P. W. Leung, C. L. Henley, and G. V. Chester, Phys. Rev. B **39**, 446 (1989).

[24] J. E. S. Socolar, Phys. Rev. B **39**, 10519 (1988).

[25] See Ref. 24, Fig. 17 [a quasiperiodic (12-fold symmetric) square-triangle-(thin)rhombus tiling].

[26] M. V. Jarić and D. R. Nelson, Phys. Rev. B **37**, 4458 (1988).

[27] As regards long-wavelength ($|\mathbf{k}| \ll 2\pi/\Lambda$) properties, the exact form of the weighting kernel $\mathcal{W}(\,)$ is unimportant beyond these three criteria [(i)–(iii)]; an adequate weighting kernel would be the two-dimensional Gaussian $\mathcal{W}(\mathbf{r}) = \exp[-|\mathbf{r}|^2/(2\Lambda^2)]/(\Lambda\sqrt{2\pi})$.

[28] V. Elser, Phys. Rev. Lett. **54**, 1730 (1985).

[29] A phase-separated (infinite) tiling is not *well behaved*; Ref. 2, subsection 10.2, broaches the issue of *modulation (in)stability* [see Fig. 9(c) (Ref. 2)]; if a system were susceptible to such an instability, phase-separated tilings would arise therein.

[30] The prefix "sub" is used to indicate the relationships that exist between the three different types of ensemble that are considered in Sec. III.

[31] The adjective "modified" is used to label objects that are associated with finite background phason strains.

[32] In the language of Appendix A, the last group on the right-hand side of Eq. (22) equals $-JB\,\mathrm{Re}[(\partial_+ h_+)^2]$, a "spin-4" object.

[33] The modified representative surface $\tilde{\mathbf{f}}(\mathbf{r})$ [see Eq. (25)] is periodic over, (i.e., single-valued on) the unit cell $\mathcal{C}$. The *modified scalar potential* $\tilde{\Phi}(\mathbf{r})$ is related to the modified representative surface by $\tilde{\mathbf{f}}(\mathbf{r}) = \nabla\tilde{\Phi}(\mathbf{r})$ [cf. Eq. (7)]. If the origin of parallel and perp. space (see Sec. II A) were fixed on a designated vertex of the four-dimensional lattice, the modified scalar potential $\tilde{\Phi}(\mathbf{r})$ would not be, for an arbitrary square-triangle approximant, single valued on the unit cell $\mathcal{C}$. The modified scalar potential $\tilde{\Phi}(\mathbf{r})$ can always be made single-valued, however, by translating the origin through a judiciously chosen perp.-space translation vector $\Delta\mathbf{f}$. That is, by making a gauge transformation $\tilde{\mathbf{f}}(\mathbf{r}) \to \tilde{\mathbf{f}}(\mathbf{r}) - \Delta\mathbf{f}$, the modified representative surface $\tilde{\mathbf{f}}(\mathbf{r})$ can be made to satisfy the gauge condition $\int_{\mathbf{G}} \tilde{\mathbf{f}}(\mathbf{r})\cdot d\mathbf{r} = 0$, where $\int_{\mathbf{G}} d\mathbf{r}$ denotes any path in parallel space whose net displacement equals any $\mathbf{G} = \sum_{ij} i\mathbf{A}^u + j\mathbf{A}^v$, both i and j are integers, and $\{\mathbf{A}^u, \mathbf{A}^v\}$ are the pair of primitive (parallel-space) translation that prescribe the unit cell $\mathcal{C}$ (see Sec. III D, second paragraph). The gauge condition can be recast as $\oint \tilde{\mathbf{f}}(\mathbf{r}) \cdot d\mathbf{r}$, where $\oint d\mathbf{r}$ denotes any closed path on the compact (toroidal) parallel space that the periodic boundary conditions of the unit cell $\mathcal{C}$ engender. Under such a gauge transformation, the phason modes $\tilde{\mathbf{h}}(\mathbf{k})$ remain invariant. (At this point, the truly inquisitive reader might wish to read Sec. IV and Appendix C, then peruse Ref. 91.) Now, the *(gauge-fixed and modified) scalar-potential field* is defined as $\tilde{\Psi}(\mathbf{r}) = \int \tilde{\Phi}(\mathbf{r}')\,\mathcal{W}(\mathbf{r}'-\mathbf{r})\,d^2\mathbf{r}'$ [cf. Eq. (26)], where the modified scalar potential $\tilde{\Phi}(\mathbf{r})$—hence $\tilde{\Psi}(\mathbf{r})$—is single valued on the unit cell $\mathcal{C}$. The *scalar-potential modes* are defined as $\tilde{\Psi}(\mathbf{k}) = (1/L)\int_{\mathcal{C}} \tilde{\Phi}(\mathbf{r}')e^{i\mathbf{k}\cdot\mathbf{r}'}d^2\mathbf{r}'$ [cf. Eq. (29)].

[34] Notwithstanding the simplifications that scalar-potential modes $\tilde{\Psi}(\mathbf{k})$ bring about [e.g., the compactness of Eq. (36) in comparison with Eq. (35)], scalar-potential modes are, in effect, nothing more than a vehicle for the constraint $k_1\tilde{h}_2(\mathbf{k}) = k_2\tilde{h}_1(\mathbf{k})$, which halves the number of independent phason modes, and which is a consequence of the irrotational property (see Sec. II B).

[35] That is, Ref. 2, Sec. 8.3.3; the reader should note that "ergodicity" (Ref. 2) and "connectivity" (this paper) are synonymous.

[36] Two Monte Carlo steps are defined in the main text of this paper; see Secs. VI A and VII D. A third Monte Carlo step is discussed in Ref. 91.

[37] K. J. Strandburg, L.-H. Tang, and M. V. Jarić, Phys. Rev. Lett. **63**, 314 (1989).

[38] Proof: Consider a square-triangle tiling, with N_v vertices, that satisfies certain (either free or periodic) boundary conditions. Now imagine the set, which comprises 2^{N_v} square-triangle tilings, which can be grown from this (the former) square-triangle tiling by way a single random-Stampfli inflation. Square-triangle tilings that lie outside of this set, but which satisfy the same boundary conditions as the square-triangle tilings that compose the set, can be found by effecting zippers of squares and triangles. Rotations of dodecagons, however, only connect the square-triangle tilings that compose the set to each other.

[39] L. S. Levitov (private communication) has found a map between (random) square-triangle tilings and configurations of domain walls on honeycomb lattices (the domain walls meet at 120° junctions); under this map, zippers correspond to the "breathing freedom" that is considered in S. N. Coppersmith, D. S. Fisher, B. I. Halperin, P. A. Lee, and W. F. Brinkman, Phys. Rev. B. **25**, 349 (1982).

[40] H. Kawamura, Physica A **177**, 73 (1991).

[41] M. Widom (private communication) has recently deduced a Bethe-ansatz solution for a subset of the transfer matrices that the map (Sec. VIII B) engenders; the subset

comprises the transfer matrices whose row states each contain as many + spins as − spins. Using this solution, he has calculated (numerically) the entropy per unit area of $[L \times \infty]$ systems as wide as $L = 1560$. By way of finite-size scaling analyzed, he obtains the following estimates: $s_v^r = 0.120055247 \pm 0.000000002$, $s_a^r = 0.129341553 \pm 0.000000002$, $K_\xi = 1.43008 \pm 0.00004$, $J = -0.9 \pm 0.1$; he cannot, as yet, estimate K_μ. Whether or not (infinite) random square-triangle tilings (at zero background phason strain) constitute an exactly solvable model [akin to the square-ice model (Ref. 43)] remains an open question.

[42] M. Widom, Phys. Rev. Lett. **70**, 2094 (1993); this clarifies, and brings up to date, Refs. 41 and 90 and some premature and/or erroneous remarks that are made in the main text of this paper.

[43] E. H. Lieb, Phys. Rev. **162**, 162 (1967).

[44] R. H. Swendsen and J.-S. Wang, Phys. Rev. Lett. **58**, 86 (1987).

[45] U. Wolff, Phys. Rev. Lett. **62**, 361 (1989).

[46] Throughout this paper, the adjectives "athermal" and "thermal" distinguish objects that do not involve (Monte Carlo) temperature from objects that do.

[47] See M. N. Barber, in *Phase Transitions and Critical Phenomena*, edited by C. Domb and J. L. Lebowitz (Academic, New York, 1983), Vol. 8, p. 145.

[48] Both F. Gähler [doctoral thesis, No. 8414, Swiss. Fed. Inst. of Tech. (ETH), Zürich, 1988] and A. P. Smith (doctoral thesis, Cornell University, Ithaca, 1990 and Ref. 49) have studied deterministic versions of Stampfli's inflation rule.

[49] A. P. Smith, *Proceedings of the Fourth International Conference on Quasicrystals*, J. Non-Cryst. **153&154**, 258 (1993).

[50] A Stampfli tiling is necessarily a random square-triangle tiling, but a random square-triangle is not necessarily a Stampfli tiling: Stampfli tilings compose a subset within the set of all (random) square-triangle tilings; non-Stampfli tilings compose the complement of this subset.

[51] D. Chandler, *Introduction to Modern Statistical Mechanics* (Oxford University Press, New York, 1987).

[52] K. Binder and D. W. Heermann, *Monte Carlo Simulation in Statistical Physics* (Springer-Verlag, Berlin, 1988).

[53] A meandering thin rhombus traces out a random walk in two dimensions. The probability that two thin rhombi annihilate after a move (viz., either an A-type or a B-type flip) is, by definition, their *annihilation cross section*. After many moves, the annihilation cross section of two thin rhombi should be more or less constant, and have a magnitude that scales proportionally to $1/L^2$, where L is the side length of the (square) $[I, D]$-type approximant in which the two thin rhombi meander. If most annihilations occur after many moves, the mean zipper length $\langle L_Z \rangle$ should thus scale proportionally to L^2. The authors stress that this argument is not rigorous. Random walks in two dimensions must be analyzed with some care: Logarithmic corrections often arise.

[54] The two halves of each symmetry-averaged phason-mode fluctuation [that is, $\langle \frac{1}{2}|\tilde{h}_i(\mathbf{k})|^2 \rangle$ and $\langle \frac{1}{2}|\tilde{h}_{i'}(\mathbf{k}')|^2 \rangle$; see Eqs. (53) and (54)] were estimated [see Eqs. (62) and (63)]; within random errors, they were always equal.

[55] A *rough* best value need not be accurate but must be, in a sense which the authors do not attempt to define, *reliable*; a reliability to within ±20% would suffice.

[56] If the starting configuration were not representative of the ensemble, and if the equilibration stage were to contain too few Monte Carlo steps, the best value $\langle q \rangle_{\mathrm{BV}}$ would suffer a systematic error.

[57] Because the fluctuation-dissipation theorem is a "standard" piece of statistical physics, Eqs. (60) and (61) are merely stated (the mathematical steps requisite to an explicit derivation are straightforward).

[58] See, for example, A. M. Tenenbaum, Y. Langsam, and M. J. Augenstein, *Data Structures Using C* (Prentice-Hall, Englewood Cliffs, NJ, 1990).

[59] An astute reader might wonder how the value of E [stage (SAMC 2)] is chosen without prior knowledge of $\tau_{\max}^{\mathrm{corr}}$ [stage (SAMC 4)]. In practice, a preliminary best value for $\tau_{\max}^{\mathrm{corr}}$ is obtained through a short athermal Monte Carlo run that uses an extremely large value of E.

[60] Such a noise floor always exists because the value of G [stage (SAMC 3)] is, in practice, always finite [note Sec. V, observation (ii)].

[61] W. H. Press, B. P. Flannery, S. A. Teukolsky, and W. T. Vetterling, *Numerical Recipes in C* (Cambridge University Press, Cambridge, England, 1988), Chap. 14, Sec. 1.

[62] M. E. J. Newman and C. L. Henley, *Proceedings of the Fourth International Conference on Quasicrystals*, J. Non-Cryst. **153&154**, 205 (1993).

[63] W. P. Orrick, senior thesis, Princeton University, 1986.

[64] By estimating total entropies for different types of unit cell (that is—for random square-triangle tilings—not just $[I, D]$-type unit cells), all of the elastic constants can, in principle, be estimated.

[65] The total entropies of ensembles that comprise $[I, D]$-type approximants were estimated using Ma's coincidence-counting method (see Sec. VII A and Appendix C), the energy method (Ref. 66) (see Sec. VII A), the histogram method (see Secs. VII B—VII F), but not the variance method (see Sec. VII A). The authors found the task of implementing the histogram method to be about as difficult (regards data structures, the propagation of random errors, etc.) as the task of implementing the thermal method, but less difficult than the task of implementing Ma's method. (The latter involved sorting and searching—see Appendix C.) Out of the three methods that were implemented, the histogram method gave, for comparable amounts of computer time, by far the smallest random errors; in other words, it was by far the most efficient.

[66] M. Oxborrow and C. L. Henley (unpublished).

[67] A. M. Ferrenberg and R. H. Swendsen, Phys. Rev. Lett. **63**, 1195 (1989).

[68] K. Binder, J. Comput. Phys. **59**, 1 (1985).

[69] S-K. Ma, J. Stat. Phys. **26**, 221 (1981).

[70] S-K. Ma and M. Payne, Phys. Rev. B **24**, 3984 (1981).

[71] S-K. Ma, *Statistical Mechanics* (World Scientific, Singapore, 1985).

[72] The number of distinct tilings that tile a (the same) unit cell grows exponentially with the cell's area. As a result, coincidences become extremely rare events for large unit cells.

[73] A caveat is that the update move and the pseudo-Hamiltonian must not engender *glassy* Monte Carlo dynamics.

[74] K. J. Strandburg and P. H. Dressel, Phys. Rev. B **41**, 2469 (1990).

[75] Consider the expectation $\langle q \rangle_L$, where q is an intensive quantity, $\langle\,\rangle$ denotes an ensemble average, and L is the system size. Suppose that estimates of $\langle q \rangle_L$ (viz.,

$[\langle q\rangle_L]_{\rm BV} \pm [\langle q\rangle_L]_{\rm RE}$) are obtained via Monte Carlo simulations for various system sizes L, where each estimate incorporates the same number of independent samples. If the ratio $[\langle q\rangle_L]_{\rm RE}/[\langle q\rangle_L]_{\rm BV}$ vanishes as $L \to \infty$, the quantity q exhibits *spatial self-averaging*. Alternatively, if the ratio $[\langle q\rangle_L]_{\rm RE}/[\langle q\rangle_L]_{\rm BV}$ remains finite as $L \to \infty$, the quantity q exhibits *lack of spatial self-averaging*.

[76] The authors confess that they do not know how much of an advantage (if any) the spatial self-averaging property of the expected energy affords the energy method, over the variance method, in practice. Random tilings exhibit long-range order in dimensions greater than two; long-range order is *marginal* (see Ref. 2) in two dimensions. Thus, the spatial self-averaging property of the expected energy should be *weak* (see Ref. 52) in dimensions greater than two and—to extend the technical language in a logical way—*marginally weak* in two dimensions.

[77] J. P. Valleau and D. N. Card, J. Chem. Phys. **57**, 5457 (1972).

[78] By using rationally related perp.-space basis vectors, as opposed to using 12-fold-symmetric (irrationally related) perp.-space basis vectors [viz., Eq. (3)], the pseudo-Hamiltonian can be rescaled (multiplication by b_I^2) so that the computation of U requires only integer arithmetic. As a result, the amount of computer time needed to perform a thermal Monte Carlo step (Sec. VII D) is less. [The use of 12-fold-symmetric perp.-space basis vectors would require floating point arithmetic, and more of it: Only if the background phason field were subtracted from the perp.-space position vector of every vertex would the pseudo-Hamiltonian be well defined (single valued).] Also, the energy level (an integer) that corresponds to a given approximant can be speedily found by subtracting the ground-state energy (an integer) from the energy of the approximant (an integer), then dividing by the energy spacing Δ (an integer). [The use of 12-fold-symmetric perp.-space basis vectors would lead to round-off errors, and necessitate the casting of floating-point numbers into integers.]

[79] Because the (flip) update moves that Orrick and Strandburg used do not conserve the average perp.-space position vector, their pseudo-Hamiltonian [i.e., Eq. (85)] engenders canonical ensembles whose specific heats remain finite as the temperature $T \to \infty$ [in this limit, the specific heat (the heat capacity per tile) of such an ensemble equals (recall the equipartition theorem; $k_B = 1$) $\frac{1}{2}d_\perp/N_t$, where $d_\perp$ is the dimension of perp. space and N_t is the number of tiles per unit cell]. Thus, the value of $[S(0)-S(\infty)]$, for any such ensemble, is infinite. In practice, however, the high-temperature offset ($\frac{1}{2}d_\perp/N_t$) in the specific heat is unobservable (that is, lost in the random error) for systems whose unit cells are large (see Figs. 3 and 4 of Ref. 10).

[80] R. J. Baxter, *Exactly Solved Models in Statistical Mechanics* (Academic, New York, 1982).

[81] Various transfer-matrix maps are described in Ref. 2, Sec. 8.5.1; see, in particular, the second column of Fig. 8 (Ref. 2).

[82] W. Li, H. Park, and M. Widom, J. Stat. Phys. **66**, 1 (1992).

[83] M. Widom, D. P. Deng, and C. L. Henley, Phys. Rev. Lett. **63**, 310 (1989).

[84] Each tiling is weighted by a factor of the form $\exp[\sum_\alpha \mu_\alpha N_\alpha]$, where α indexes *tile type*, μ_α is the chemical potential for tile type α, and N_α is the number of tiles in the tiling of tile type α. (Tile type distinguishes both shape and orientation.) If tile types α_1 and α_2 are related by a symmetry operation, μ_{α_1} and μ_{α_2} can be identified; as a result, only a few independent chemical potentials $\mu_\alpha^{\rm ind}$ exist. These are adjusted until the longitudinal background phason strain vanishes; the grand canonical ensemble of spin configurations is then equivalent to the maximally random ensemble at zero background phason strain.

[85] H. Kawamura, Prog. Theor. Phys. **63**, 24 (1980).

[86] The efficiencies of various transfer-matrix maps are compared quantitatively in Ref. 2, Sec. 8.5.2 (the rightmost column of Fig. 8).

[87] A sequence is a realization of a row-state; a "row state" and a "sequence" thus connote the abstract and concrete aspects, respectively, of the same entity.

[88] L. J. Shaw and C. L. Henley, J. Phys. A **24**, 4129 (1991).

[89] If chemical potentials $\mu_\alpha^{\rm ind}$ (see Ref. 84) were introduced, they would be found unable to control the background phason strain (all *fugacity* terms would factor out of the transfer matrix).

[90] Under the constraint that the background phason strain $\underline{B}$ takes the form of Eq. (19), which corresponds to both the existence of as many positive domain walls as negative domain walls (see Sec. VIII C, last paragraph) and the absence of (symmetry-breaking) chemical potentials, the entropy per unit area in the infinite-system (thermodynamic) limit, up to third order in $\underline{B}$, is [see Eq. (13)] $s_a^r[B] \equiv \sigma[\underline{E} \to \underline{B}] = s_a^r - \frac{1}{2}K_\xi B^2 - \frac{8}{6}JB^3$. Widom uses a finite-size scaling form that incorporates $s_a^r[B]$, and thereby obtains estimates of s_a^r (s_v^r), K_ξ, and J.

[91] In the athermal Monte Carlo runs (see Sec. VI E) that were performed, scalar-potential modes $\tilde\Psi(\mathbf{k}) = (1/L)\int_{\mathcal{C}} \tilde\Phi(\mathbf{r})e^{i\mathbf{k}\cdot\mathbf{r}'}\,d^2\mathbf{r}'$ [see Eq. (33)] were never calculated directly from the modified scalar potential $\tilde\Phi(\mathbf{r})$; the value of $\tilde\Phi(\mathbf{r})$ at each vertex ($\mathbf{r} = \mathbf{r}_v$) was neither determined nor updated. [Phason modes $\tilde{\mathbf{h}}(\mathbf{k})$ were instead calculated by using Eq. (57). Note that scalar-potential modes $\tilde\Psi(\mathbf{k})$ are related to phason modes $\tilde{\mathbf{h}}(\mathbf{k})$ by Eq. (33)]. Thus, whether or not, at any particular instant of Monte Carlo time, the (never-calculated) modified scalar potential $\tilde\Phi(\mathbf{r})$ was single valued on the unit cell $\mathcal{C}$ (see Ref. 33), given the designated vertex of the four-dimensional lattice that served as the (fixed) origin of parallel and perp. space (see Sec. II A) is a moot question. Nevertheless, consider a (hypothetical) Monte Carlo step, based on the zipper update move (Sec. IV), for which the modified scalar potential $\tilde\Phi(\mathbf{r})$ is calculated and kept single valued by making a gauge transformation $\tilde{\mathbf{f}}(\mathbf{r}) \to \tilde{\mathbf{f}}(\mathbf{r}) - \Delta\mathbf{f}$ (see Ref. 33). With such a Monte Carlo step, the requisite perp.-space translation vector $\Delta\mathbf{f}$, for a given realization of the zipper update move, would depend only on the homology (i.e., the winding numbers) of the zipper that is effected. For a *simple* zipper, i.e., a zipper whose homology is trivial (both windings numbers are zero), $\Delta\mathbf{f}$ would equal zero. Thus, provided that the modified scalar potential of the starting configuration were single valued, the need for gauge transformations could be eliminated by prohibiting every realization of the zipper update that effects a *complex* zipper, i.e., a zipper whose homology is nontrivial (at least one winding number is nonzero). Such a tactic, however, would reduce the efficiency of the Monte Carlo step (most realizations would be *vetoed*); furthermore, the connectivity (see Sec. IV) of the "simple-zipper-only" update move might

be less than the connectivity of the "any-zipper" update move; the authors do not fully understand, and have not pursued, these subtleties. Now, a complex zipper changes the sum (modified–rationally-related) perp.-space position vector of the vertices within an $[I, D]$-type unit cell (see Appendix C). The second stage of the "coincidence-counting athermal Monte Carlo step" (Ref. 33) constitutes a gauge transformation that is identical in spirit to (though different in a few technical details from) the above gauge transformation $[\tilde{\mathbf{f}}(\mathbf{r}) \rightarrow \tilde{\mathbf{f}}(\mathbf{r}) - \Delta\mathbf{f}]$. [The second stage of the coincidence-counting athermal Monte Carlo step translates the origin through an integral combination of four-dimensional basis vectors, that is, the origin saltates through both perp. and parallel space, but always lands on a vertex of the four-dimensional regular lattice. As a result, the four-dimensional position of every vertex can always be specified by four integers; this feature facilitates the coincidence-counting athermal Monte Carlo step's implementation.]

[92] H. Park and M. den Nijs, Phys. Rev. B, **38**, 565 (1987).
[93] H. Park and M. Widom, J. Stat. Phys. **61**, 51 (1990).
[94] V. Privman, in *Finite Size Scaling and Numerical Simulations of Statistical Systems*, edited by V. Privman (World Scientific, Singapore, 1990).
[95] T. Ishimasa, H.-U. Nissen, and Y. Fukano, Phys. Rev. Lett. **55**, 511 (1985).
[96] T. Ishimasa, H.-U. Nissen, and Y. Fukano, Philos. Mag. A **58**, 835 (1988).
[97] H. Chen, D. X. Li, and K. H. Kuo, Phys. Rev. Lett. **60**, 1645 (1988).
[98] C. Beeli, F. Gähler, H.-U. Nissen, and P. Stadelmann, J. Phys. (Paris) **51**, 661 (1990).
[99] K. H. Kuo, Y. C. Feng, and H. Chen, Phys. Rev. Lett. **61**, 1740 (1988).
[100] Z. M. Wang, Q. B. Yang, and K. H. Kuo, Acta Crystallogr. A **45**, 268 (1989).
[101] M. Mihalkovič and P. Mrafko (private communication).